BIOACTIVE AND ELASTOMERIC SCAFFOLDS: A GROWTH-FACTOR-FREE APPROACH FOR BONE TISSUE ENGINEERING

A THESIS

by

PUNYAVEE KERATIVITAYANAN

Submitted to the Office of Graduate and Professional Studies of
Texas A&M University
in partial fulfillment of the requirements for the degree of

MASTER OF SCIENCE

Chair of Committee,	Akhilesh Gaharwar
Committee Members,	Daniel Alge
	Melissa Grunlan
Head of Department,	Gerald L. Cote

December 2015

Major Subject: Biomedical Engineering

ABSTRACT

Bone is the second most transplanted organ following blood, and significant advances have been made in developing synthetic bone graft substitutes and scaffolds. However, there remains a critical need for osteoinductive scaffolds with mechanical functionality for bone tissue engineering at load-bearing sites. Here, we reported nanocomposite scaffolds of elastomeric poly(glycerol sebacate)(PGS) and osteoindictive nanosilicates, fabricated via salt-leaching method. Nanosilicates are ultrathin nanomaterials reported to induce osteogenic differentiation of human stem cells in the absence of any osteogenic factors such as dexamethasone or bone morphogenetic proteins-2 (BMP2). The addition of nanosilicates to PGS matrix resulted in enhanced physical integrity as well as increased mechanical strength and toughness. Remarkably, elastomeric properties of the scaffolds were not compromised, providing a load-transducing environment for bone regeneration. PGS/nanosilicates scaffolds supported cell proliferation and promoted cell spreading. The addition of nanosilicates upregulated osteogenic differentiation of seeded preosteoblasts in a concentration-dependent manner as evidenced by increased ALP activity and matrix mineralization, even when cultured in normal growth media without any osteogenic factors. All in all, the combination of elasticity and tunable stiffness, tailorable degradation profiles, and the ability to promote osteogenic differentiation of the scaffolds offered a promising growth-factor-free approach for bone tissue engineering.

ACKNOWLEDGEMENTS

This dissertation would not have been plausible without the guidance and the help of several individuals who contributed their valuable time and assistance throughout my master thesis.

I owe my deepest gratitude to my supervisor, Dr. Akhilesh Gaharwar for his guidance and support throughout the course of this research. Thanks also my committee, Dr. Daniel Alge and Dr. Melissa Grunlan for their time and advice.

I also would like to thank my colleagues in Dr. Gaharwar research group who gave me ideas, suggestions, and help.

Lastly, I would like to thank those who supported me in any aspects during the completion of this project and dissertation. And I would like to apologize to those whose names are not mentioned in this acknowledgement.

NOMENCLATURE

ALP	Alkaline Phosphatase
ARS	Alizarin Red S
ATR-FTIR	Attenuated Total Reflectance – Fourier Transform Infrared Spectroscopy
BSA	Bovine Serum Albumin
DPBS	Dulbecco's Phosphate Buffered Saline
FBS	Fetal Bovine Serum
nSi	Nanosilicates
PGS	Poly(glycerol sebacate)
PBS	Phosphate Buffer Saline
SBF	Simulated Body Fluid
SDS	Sodium Dodecyl Sulfate
SEM	Scanning Electron Microscopy
TGA	Thermogravimetric Analysis
THF	Tetrahydrofuran

TABLE OF CONTENTS

Page

ABSTRACT ii

ACKNOWLEDGEMENTS iii

NOMENCLATURE iv

TABLE OF CONTENTS v

LIST OF FIGURES vii

CHAPTER I INTRODUCTION 1

CHAPTER II MANUSCRIPT#1: ELASTOMERIC AND MECHANICALLY STIFF NANOCOMPOSITES FROM POLY(GLYCEROL SEBACATE) AND BIOACTIVE NANOSILICATES 6

II.1 Overview 6
II.2 Materials and Methods 7
II.2.1 Poly(glycerol sebacate)(PGS) synthesis 7
II.2.2 Synthesis of PGS and PGS-nanosilicate composites 7
II.2.3 Surface morphology 7
II.2.4 Sol content analysis 8
II.2.5 Hydration properties 9
II.2.6 Degradation studies 9
II.2.7 Thermal analysis 9
II.2.8 Mechanical properties 10
II.2.9 *In vitro* biomineralization 10
II.2.10 Protein adsorption 11
II.2.11 *In vitro* cell adhesion, proliferation, and differentiation 11
II.2.12 Statistics 13
II.3 Results and Discussion 13
II.3.1 Nanosilicates enhanced crosslinking density and hydrophilicity of nanocomposites 13
II.3.2 Nanosilicates improved physiological stability of nanocomposites 16
II.3.3 Nanosilicates enhanced thermal stability of nanocomposites 18
II.3.4 Nanosilicates enhanced mechanical stiffness of nanocomposites 18
II.3.5 Nanosilicates enhanced *in vitro* bioactivity 22
II.3.6 Nanosilicates enhanced cell adhesion and proliferation 24
II.3.7 Differentiation of preosteoblasts on PGS and PGS-nSi 27
II.4 Summary 28

Page

CHAPTER III MANUSCRIPT#2: ELASTOMERIC POLY(GLYCEROL SEBACATE)/NANOSILICATES SCAFFOLDS: A GROWTH-FACTOR-FREE APPROACH FOR BONE TISSUE ENGINEERING 29

III.1 Overview 29
III.2 Materials and Methods 30
III.2.1 Poly(glycerol sebacate)(PGS) synthesis 30
III.2.2 Fabrication of PGS and PGS-nanosilicates (PGS-nSi) scaffolds 32
III.2.3 Surface and cross-section morphology 32
III.2.4 Degradation studies 33
III.2.5 Mechanical properties 33
III.2.6 Protein adsorption 33
III.2.7 Cell culture and *in vitro* cell adhesion 34
III.2.8 *In vitro* cell proliferation and differentiation 35
III.2.9 Statistics 35
III.3 Results and Discussion 36
III.3.1 Microstructure of PGS/nanosilicates scaffolds 36
III.3.2 Nanosilicates enhanced physical stability of the scaffolds 38
III.3.3 Nanosilicates increased mechanical stiffness without compromising elastomeric properties 40
III.3.4 PGS/nanosilicates scaffolds were protein adhesive 43
III.3.5 PGS/nanosilciates scaffolds enhanced cell adhesion and supported cell proliferation 44
III.3.6 PGS/nanosilicates scaffolds promoted osteogenic differentiation ... 47
III.4 Summary 50

CHAPTER IV CONCLUSIONS 51

REFERENCES 53

LIST OF FIGURES

FIGURE		Page
II.1	Synthesis and fabrication of PGS nanocomposites	8
II.2	Effects of nanosilicates on crosslinking density and hydrophilicity	15
II.3	Effects of nanosilicates on degradation	17
II.4	Effects of nanosilicates on thermal properties	19
II.5	Effects of nanosilicates on mechanical properties	21
II.6	*In vitro* bioactivity of nanocomposites	23
II.7	Cellular adhesion and proliferation on nanocomposites	24
II.8	Differentiation of preosteoblasts on PGS nanocomposites	26
III.1	PGS synthesis and PGS/nanosilicates networks	30
III.2	Porous scaffolds fabrication procedure	31
III.3	PGS and PGS-nSi porous scaffolds	37
III.4	Scaffold degradation in 0.01M NaOH over a week	38
III.5	Mechanical properties	41
III.6	Protein adsorption and cell adhesion on PGS/nanosilicates scaffolds	43
III.7	Cell adhesion and proliferation	45
III.8	Alkaline phosphatase (ALP) expression	48
III.9	Matrix mineralization	49

CHAPTER I

INTRODUCTION

Over 2.2 million bone grafting operations are performed worldwide annually, at an approximate cost of 2.5 billion USD, making bone the second most transplanted organs following blood. With increasing aging population, the occurrence of bone injuries and degeneration is on the rise.[1, 2] Posttraumatic complications such as non-unions, mal-unions, and delayed unions pose additional challenges.[1] Autograft is the clinical gold standard as it provides optimal osteogenesis. However, the operation at the donor site can increase recovery time and risk of complications. It has been reported that harvesting autologous bone is associated with 8.5-20% post-operation complications, including blood loss, hernia formation, nerve injury, infection, for instance. In addition, there is a limited supply of bone that can be harvested, especially for elderly or paediatric patients, and those with malignant diseases.[1, 3-5] Allograft is the surgeon's second choice, and its used has been increased for 15-fold in the past decade. However, its efficiency in inducing bone regeneration is lower compared to autograft. It is also immunogenic and carries the risk of disease transmission.[1, 6-10] Allograft processing, including freezing and irradiation, can mitigate these risks, but at the same time weaken its mechanical and biological properties. Demineralized bone matrix (DBM) is another available option. Demineralization process does not completely eradicate bone growth factors, making it more osteinductive than conventional processed allograft. However, its clinical results are not constantly good, partially attributed to non-uniform processing procedures. Consequently, DBM is mostly used as bone graft extender rather than sole bone graft substitute.[1, 6-10] Due to aforementioned limitations, there is a rising demand for synthetic bone graft substitutes.

Essential biological characteristic of an ideal bone graft substitute are osteoconduction, osteoinduction, and osteointegration. Osteoconduction is when bone grows on the surface or along bone-material interface. It usually involves facilitation and orientation

of blood vessels, and formation of new Harversian systems. An osteoconductive surface permits bone to grow on its surface or into the pores or channels. On the other hand, osteoinduction means stimulation of primitive undifferentiated cells to develop into bone-forming cell lineage. Some define it as the process which osteogenesis is induced. And osteintegration is the bonding between grafting materials and host bone.[1, 11]

Macroporous bioactive ceramic granules are the most popular amongst synthetic bone grafts and bone graft extensions currently available in the market. Surgeons mix them with patient's blood and use as a putty to fill bone defects.[6-10] Synthetic hydroxyapatite (sHA), beta tricalcium phosphate (β-TCP), and biphasic calcium phosphate (a mixture of β-TCP and sHA) are the most commonly used as sHA has a stoichiometry similar to a natural bone mineral (calcium-deficient hydroxyapatite, CDHA) whereas β-TCP is stoichiometrically similar to amorphous bone precursors.[9] However, these materials are osteoconductive but not osteoinductive. In addition, sHA undergoes slow resorption, sometimes too slow for bone regeneration application where grafting materials need to be ultimately replaced by newly formed bone. Remodeling of sHA is not as efficient as that of natural bone mineral which contains 4-5% of carbonate, magenesium, strontium, and fluoride ions. Incorporation of carbonate and silicon has been shown to enhance degradation rate and bioactivity of sHA, but it is still not ideal.[12] Ultraporous β-TCP was developed to mimic the structure of trabecular bone, but like sHA, it does not possess intrinsic osteogenic properties.[1] It degrades faster than sHA, and completely resorbed in 6-18 months. However, it was reported that in most cases, volume of newly formed bone was less than that of resorbed β-TCP.[13]

In the past few years, bioactive glasses have gained increasing interests in bone tissue engineering research. They are osteoinductive silica-based materials composed of Na_2O-CaO-P_2O_5-SiO_2. Compared to sHA, bioactive glasses exhibit 10-fold higher bioactivity index, indicating significantly more superior bone bonding ability. They are classified as class A biomaterials, which means they can stimulate bone growth, and strongly bond to both bone and soft tissues. Nevertheless, translational success of bioactive glasses has

been restricted by their brittleness and complex chemistry.[9, 10, 14, 15] Therefore, there is a need for alternative materials.

In this regard, Gaharwar *et al.* recently reported the ability of nanosilicates (Laponite - $Na^{+}_{0.7}[(Mg_{5.5}Li_{0.3})Si_8O_{20}(OH)_4]^{-}_{0.7}$) to induce osteogenic differentiation of adipose stem cells (ACSs) and human mesenchymal stem cells (hMSCs) in the absence of any osteoinductive supplements such as dexamethasone and bone morphogenic protein-2 (BMP-2).[15, 16] Nanosilicates dissociate into Na^{+}, Mg^{2+}, Li^{+}, and $Si(OH)_4$ in aqueous solution; and these ionic dissolution products are contributing to their osteoinductive properties. Specifically, magnesium ions ($Mg^{2+)}$ were reported to promote adhesion of osteoblasts to material surfaces via fibronectin receptor $\alpha_5\beta_1$ and β_1 integrins, which brought about enhanced gene expression of ECM proteins and formation of new bone.[17, 18] Lithium ions (Li^{+}) were found to activate Wnt/β-catenin signaling pathway which stimulated osteogenic differentiation of mesenchymal progenitor cells, promoted cell proliferation and mineralization, while inhibited apoptosis and osteoclastogenesis. [19] Orthosilicic acid ($Si(OH)_4$) also stimulated osteogenic differentiation as well as promoted collagen type I synthesis.[17, 20] Moreover, nanosilicates presented cytotoxicity at ten-fold higher concentration comparing to silica nanoparticles and sHA.[15] Possessing these properties, nanosilicates offer a growth-factor free approach for bone regeneration, minimizing complexities and expenses involved in growth factor delivery. It should be noted that the majority of newly formed bone come from undifferentiated cells that are induced to preosteoblasts. Therefore, osteinduction capability of scaffolds is of utmost importance for proper bone repair and anchorage of the grafts.[11]

Since nanosilicates have heterogenous charge distribution, they interact strongly with hydrophilic polymers such as poly(ethylene glycol)(PEG) and collagen. The resulting nanocomposites displayed unique property combinations which are promising for biomedical applications.[21, 22] Examples are high performance elastomers[23-26], moldable hydrogels[27], injectable hemostats[28], self-healing structures[29], and drug

delivery vehicles[30, 31]. Our group recently reported that incorporation of nanosilicates in collage-based hydrogels gave rise to four-fold increase in osteogenesis in the absence of any osteoinductive factors.[32] However, development of osteoinductive scaffolds which load-transducing mechanical properties remains as a significant challenge. It is important to note that bone is a dynamic tissue where remodeling continuously takes place. Applied loads play critical roles in determining the rate of turnover as well as the formation of callus, its volume, and stiffness during bone healing. Thus, scaffolds with tailorable mechanical properties and degradation kinetics are of pivotal importance.

Here, we report the fabrication and performance of nanocomposite scaffolds made from poly(glycerol sebacate)(PGS) and nanosilicates. PGS is tough biodegradable elastomeric polyester.[33-35] It undergoes surface erosion, making it preferable for scaffolding applications compared to other polyesters. Its degradation products are also completely resorbable.[33, 35, 36] PGS was demonstrated to trigger less inflammatory responses and minimal fibrous encapsulation compared to other widely used synthetic polymers such as poly(lactic acid)(PLA) and poly(lactic-co-glycolic acid)(PLGA)-based materials.[33-35] Also, mechanical properties of PGS are tunable by varying crosslinking conditions, functionalization, and incorporation of fillers.[37] Thus, it is expected that porous PGS/nanosilicates scaffolds would provide optimal load-transducing environment for bone regeneration.

In addition to elastomericity and tunable mechanical properties, PGS was reported to be a promising osteoconductive substrate that supported phenotypes of osteoblasts *in vitro*.[38] An in vivo study showed that PGS promoted healing of a critical size defect in rabbits. Tomography and mechanical testing at 8 weeks post implantation suggested that its elasticity provided a load-transducing environment in which osteogenesis, matrix deposition, and bone maturation could take place.[37] Furthermore, PGS could induce angiogenic differentiation of bone marrow mononuclear cells, contributing to its extensive studies as vascular graft. Since angiogenesis is generally coupled with osteogenesis, this property stresses its potential for bone tissue engineering.[37, 39]

Since PGS has been shown to be osteoconductive, its action is expected to complement the osteoinduction capability of nanosilicates, resulting in more complete bone repair.

Our objective is to develop osteoinductive scaffolds that provide load-transducing environment suitable for bone tissue engineering. Here, we propose PGS/nanosilicate porous scaffolds fabricated via salt-leaching method. Nanosilicates are osteoinductive, offering a growth-factor free approach for bone tissue engineering. PGS is expected to provide further osteoinduction and load-transducing environment. We anticipate that PGS/nanosilicates scaffolds will have osteoinduction capability and tunable mechanical functionality, promising for bone tissue engineering.

CHAPTER II*

MANUSCRIPT#1: ELASTOMERIC AND MECHANICALLY STIFF NANOCOMPOSITES FROM POLY(GLYCEROLSEBACATE) AND BIOACTIVE NANOSILICATES

II.1 OVERVIEW

Poly(glycerol sebacate) (PGS) has been proposed for tissue engineering applications owing to its tough elastomeric mechanical properties, biocompatibility and controllable degradation. However, PGS shows limited bioactivity and thus constraining its utilization for musculoskeletal tissue engineering. To address this issue, we developed bioactive, highly elastomeric, and mechanically stiff nanocomposites by covalently reinforcing PGS network with two-dimensional (2D) nanosilicates. Nanosilicates are ultrathin nanomaterials and can induce osteogenic differentiation of human stem cells in the absence of any osteogenic factors such as dexamethasone or bone morphogenetic proteins-2 (BMP2). The addition of nanosilicate to PGS matrix significantly enhances the mechanical stiffness without affecting the elastomeric properties. Moreover, nanocomposites with higher amount of nanosilicates have higher *in vitro* stability as determined by degradation kinetics. The increase in mechanical stiffness and *in vitro* stability is mainly attributed to enhanced interactions between nanosilicates and PGS. We evaluated the *in vitro* bioactivity of nanocomposite using MC-3T3 preosteoblast cells. The addition of nanosilicates significantly enhances the cell adhesion, support cell proliferation, upregulate alkaline phosphates and mineralized matrix production. Overall, the combination of high mechanically stiffness and elastomericity, tailorable degradation profile, and the ability to promote osteogenic differentiation of PGS-nanosilicate can be used for regeneration of bone.

---

*Reprinted with permission from Kerativitayanan P, Gaharwar AK. Elastomeric and mechanically stiff nanocomposites from poly(glycerol sebacate) and bioactive nanosilicates. Acta Biomaterialia 2015;26:34-44.

II.2 MATERIALS AND METHODS

II.2.1 Poly(glycerol sebacate)(PGS) Synthesis

Poly(glycerol sebacate)(PGS) was synthesized by polycondensation of glycerol and sebacic acid (figure II.1a) according to previously published methods. Glycerol ($C_3H_8O_3$) and sebacic acid ($C_{10}H_{18}O_4$) were obtained from Sigma-Aldrich (USA). Briefly, glycerol and sebacic acid in an equimolar ratio were mixed in a two-neck round-bottom flask, and heated to 120°C under nitrogen for 24 hours. The pressured was then gradually decreased to 50mTorr, and the reaction was continued for 48 hours. The vacuum was turned off and the reactor was filled with Argon. The pre-polymer solution was cooled down to room temperature, transferred to a glass container, and kept in 4°C refrigerator for future use.

II.2.2 Synthesis of PGS and PGS-nanosilicate Composites

Nanosilicate (Laponite XLG) was obtained from BYK Additives Inc. The nanocomposites were prepared by mixing PGS pre-polymer in 70% chloroform-30% ethanol (50%w/v), then adding 0%, 1%, 2.5%, 5%, 10%, 15% w/w of nanosilicates to the PGS (figure II.1b). Nanosilicates (nSi) were suspended in the solution using a probe sonicator (Model FB120, Fisher Scientific) to uniformly disperse it in PGS prepolymer solution. The increase in viscosity was observed as we add nanosilicates to PGS indicating enhanced interactions between nanoparticle and PGS prepolymer. Then, the solution was poured into a teflon mold and left in a fume hood for 48 hours for solvent evaporation. The dried pre-polymer was put in a vacuum dessicator for 24 hours before thermal curing in a vacuum oven at 130°C for 48 hours. The samples were named PGS, PGS-1%nSi, PGS-2.5%nSi, PGS-5%nSi, PGS-10%nSi, and PGS-15%nSi, respectively, according to concentration of nanosilicates.

II.2.3 Surface Morphology

The surface morphology of the nanocomposites was imaged using scanning electron microscopy (FEI Quanta 600 FE-SEM, USA, fitted with an Oxford EDS system). The

nanocomposite samples were vacuum dried in a dessicator, then sputter coated with Au/Pd up to a thickness of 8 nm before being mounted onto the specimen stub with carbon tape.

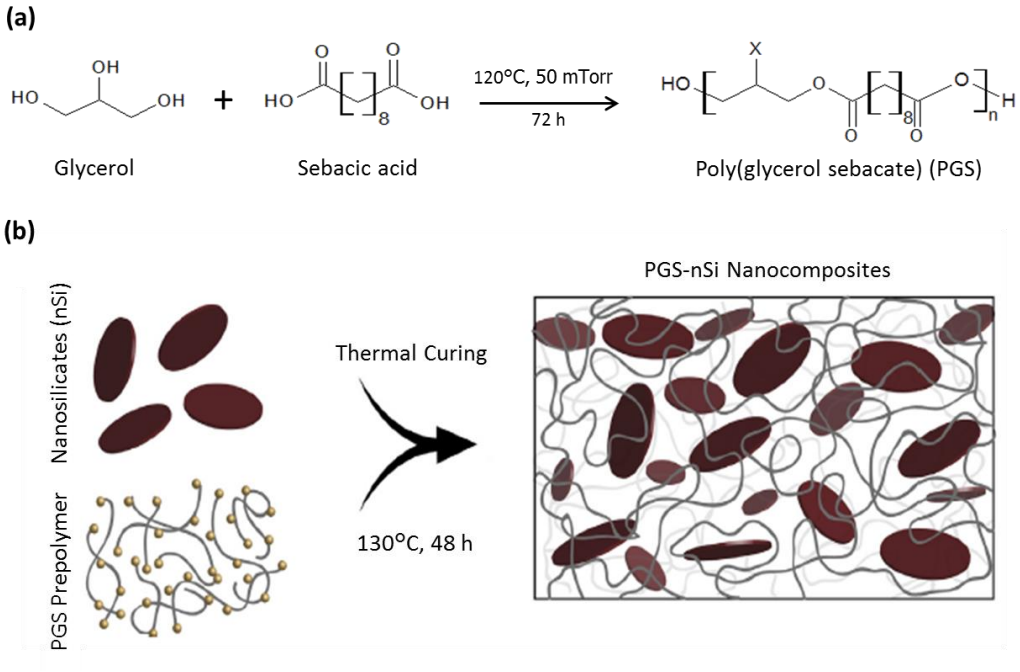

Figure II.1 Synthesis and fabrication of PGS nanocomposites. (a) PGS was synthesized via polycondensation of glycerol and sebacic acid. (b) The prepolymer containing PGS and nanosilicate were thermally crosslinked to obtain elastomeric nanocomposites.

II.2.4 Sol Content Analysis

Degree of crosslinking was determined by sol (uncrosslinked network) and gel (crosslinked network) content analysis. Nanocomposites were submerged in THF for 24 hours. The swollen samples were dried overnight and the final weight (W_d) was measured. The percentage of sol content (sol%) was calculated from the initial (W_i) and final weight (W_d) using equation II.1.

$$\text{Sol (\%)} = \frac{W_i - W_d}{W_i} \times 100 \qquad \text{(Equation II.1)}$$

II.2.5 Hydration Properties

Hydration properties of nanocomposites were evaluated from swelling ratio and contact angle measurement. For the swelling study, samples were submerged in phosphate buffer saline (PBS) at 37°C for 48 hours. The excess surface water was drained and the weight of swollen samples (W_s) was measured. The swelling ratio was calculated from the swollen (W_s) and initial weight (W_i) using equation II.2. Surface hydrophilicity was determined by water contact angle analysis. A drop of water was dripped onto the sample using a 21-gauge flat needle. The shape of the water drop was captured with a camera (KSV CAM-200 contact angle analyzer, KSV Instruments LTD), and the contact angle was analyzed using imageJ software.

$$\text{Swelling ratio} = \frac{W_s}{W_i} \qquad \text{(Equation II.2)}$$

II.2.6 Degradation Studies

Nanocomposites were submerged in phosphate buffer saline (PBS) at 37°C. The samples were collected after 3,7,10, and 28 days, and dried weight was determined. Percentage of weight loss at specific time point was calculated from the initial (W_i) and final dried weight (W_d) using equation II.3. In complementary to weight loss, surfaces of nanocomposites before (day 0) and after 28 days in PBS (day 28) were imaged using scanning electron microscopy (SEM) (Neoscope JCM-5000).

$$\text{Weight loss (\%)} = \frac{W_i - W_d}{W_i} \times 100 \qquad \text{(Equation II.3)}$$

II.2.7 Thermal Analysis

Thermal properties of nanocomposites were determined by thermogravimetric analysis (TGA) (TGA Q50, TA Instruments). The samples weighed ≈10 mg were heated from 0°C to 750°C with the heating rate of 10°C min^{-1}. Thermal stability was determined by

calculating the remaining weight at 750°C. Degradation temperature and temperature range were determined from the first derivative curve (% weight loss/°C).

II.2.8 Mechanical Properties

Since we aimed to use the nanocomposites for bone regeneration at load bearing sites, samples were subjected to cyclic compression using the eXpert 7600, ADMET, USA). Five cycles of loading and unloading were implemented (strain rate 0.1 mm/min). Stress-strain curves were plotted, and compressive modulus, energy loss, and percentage of recovery were calculated. For the fractured surface study, nanocomposites were cut into a thin strip (2 cm long x 0.5 cm wide x 1 mm thick) and pulled vertically (strain rate 0.1 mm/min) until fractured. The fractured surfaces were imaged using scanning electron microscopy to study surface characteristics.

II.2.9 *In vitro* Biomineralization

Bone bioactivity of nanocomposites was studied by submerging samples in 10X simulated body fluid (10X SBF). SBF was prepared according to previously published methods.[40] Nanocomposites were punched using a 6mm diameter biopsy punch. The samples were weighed and the volume of SBF needed was calculated accordingly (150mg/100ml SBF). The samples were immersed in 10X SBF for 30 minutes and 6 hours, then air dried for further studies. Attenuated Total Reflectance – Fourier Transform Infrared Spectroscopy (ATR-FTIR) (Bruker Alpha FTIR) was used to determine characteristic bands of hydroxycarbonate apatite layer formed on the surface. The samples were further imaged using scanning electron microscopy (SEM). In addition, they were stained by Alizarin Red S (ARS) (2% solution, pH 4.2, Electron Microscopy Sciences) for calcium deposit, and imaged using a stero microscope (Amscope FMA 050). For quantitative analysis, the stained samples were washed in 10% acetic acid (Fisher Scientific) for 30 minutes with shaking. The solution was neutralized with 10% ammonium hydroxide (Sigma-Aldrich) until the pH fell within the range of 4.1-4.5, then the UV absorbance was read at 405nm (Infinite M200PRO,

TECAN). The absorbance was converted to ARS concentration using a predetermined standard curve.

II.2.10 Protein Adsorption

Protein adsorption on the nanocomposites was determined by washing the samples (6mm diameter) twice with Dulbecco's phosphate buffered saline (DPBS) before soaking in 10% fetal bovine serum (FBS) at 37°C for 24 hours. DPBS and FBS were purchased from Life Technologies. The samples were washed thrice with DPBS to remove non-specifically adsorbed proteins. Then, 2% sodium dodecyl sulfate (SDS) solution (20% SDS solution, Amresco) was added with shaking for 6 hours to collect adhered protein. The solution was collected and protein concentration was quantified using a Micro BCA™ Protein Assay Kit (Thermo Scientific). Briefly, an equal amount of collected supernatant and BCA working reagent were incubated at 37°C for 2 hours then quantified using a UV/Vis spectrophotometer at 562nm. The bovine serum albumin (BSA) came with the assay kit was used as a standard.

II.2.11 *In vitro* Cell Adhesion, Proliferation and Differentiation

MC-3T3 E1 preosteoblasts (ATCC®) were cultured in normal growth media (α-MEM) (Hyclone^{TM}) containing 10% fetal bovine serum (FBS) and 1% penicillin/streptomycin (gibco® by Life Technologies), at 37°C in an incubator with humidified atmosphere (5% CO_2). The cells were used for seeding at 70% confluency in culture. Nanocomposites (6mm diameter) were glued to a glass slide (1x1cm) with a medical grade silicone adhesive (Loctite 5240), and put into a 24 well plate. The glass slide would aid in handling the samples without disturbing adhered cells. Before cell seeding, the samples were washed twice with DPBS, sterilized under UV light for 4 hours, and incubated in normal growth media overnight at 37°C. The cells were typsinized (0.5% trypsin-EDTA, gibco® by Life Technologies) and seeded on the samples at the high density of $1x10^5$ cells in 5µl normal growth media. The seeded samples were incubated at 37°C for 3 hours to allow cells to adhere; then, 600µl of normal growth media was added. The samples were collected at 24 hours and 3 days after the initial cell seeding. They were

washed with DPBS, fixed with 2.5% glutaraldehyde (25% aqueous solution, Alfa Aesar®), and dehydrated with graded ethanol (30%, 50%, 75%, 95%, and 100%, respectively). The seeded samples were then subjected to chemical drying with hexamethyldisilazane (HDMS) (electronic grade, Alfa Aesar®) before sputter coated and imaged with scanning electron microscope.

Preosteoblasts were typsinized and seeded on pre-conditioned samples at the density of 5,000 cells per sample per well (96 well plate) in normal growth media. The samples were divided into 2 sets, the first set was cultured in normal growth media while the other in osteoconductive media (α-MEM supplemented with 10mM β-glycerolphosphate and 0.05mM ascorbic acid). β-glycerolphosphate and ascorbic acid were used as purchased from Sigma-Aldrich. Osteoconductive media was added to the second set of samples at 24 hours after the initial cell seeding. Cell proliferation at day 1, 5, 7, 10, and 14 was determined by alamarBlue® assay (Thermo Scientific) following the standard manufacturer's protocol.

Osteogenic differentiation of preosteoblasts was evaluated from determining production of alkaline phosphatase (ALP) and matrix mineralization. ALP was stained by BCIP/NBT solution (Thermo Scientific) at day 3 following the standard manufacturer's protocols. ALP activity was further quantified using SensoLyte® *p*NPP Alkaline Phosphatase Assay Kit, and normalized by amount of double strand DNA (ds-DNA). The amount of dsDNA was quantified using PicoGreen® Assay in conjunction with NanoDrop3300 fluorospectrometer (Thermo Scientific). In addition, matrix mineralization at day 14 was stained by Alizarin Red S, and imaged with the steromicroscope. The stained images were quantified for the area coverage using ImageJ (NIH) software with Threshold_Colour plugin. For all studies, seeded cells were cultured in normal growth media and osteoconductive media for comparison.

II.2.12 Statistics

The experimental results are plotted as mean ± standard deviation (n=3-5). Statistical analysis of all quantitative data was performed by one-way analysis of variance (ANOVA), while pair-wise comparison of data was determined by Turkey's post hoc test. Statistical significance was shown as *$p < 0.05$, **$p < 0.01$, ***$p < 0.001$.

II.3 RESULTS AND DISCUSSION

PGS prepolymer was synthesized via polycondensation of glycerol and sebacic acid with molecular weight (Mw) ~ 5012 Da and polydispersity index (PDI) of ~ 2.6, according to previously published protocol.[41] A fully crosslinked PGS polymer was obtained by thermal curing process at 130°C for 48 h, according to previously published reports. Different amount of nanosilicates (0%, 1%, 2.5%, 5%, 10%, 15% w/w to the PGS) was incorporated before the thermal crosslinking process to obtain PGS-nanosilicate composites. All the samples were used to evaluate physical and chemical characterization without any post-modification process.

II.3.1 Nanosilicates Enhanced Crosslinking Density and Hydrophilicity of Nanocomposites

The degree of covalent crosslinking after thermal curing process was determined *via* sol-gel contents. Covalently crosslinked nanocomposites readily swelled in THF and the sol content was leached out. The remaining dry weight of crosslinked network was used to determine the gel content of the nanocomposite network. The results showed that the amount of sol content (uncrosslinked macromer) decreased with increasing nanosilicate concentration, indicating the increase in crosslinking density (figure II.2a). For example, the sol content was decreased by 15.5% upon the addition of 5% nanosilicates. This ascertained the role of nanosilicates as multifunctional crosslinkers as previously reported.[24, 27] Although the exact nature of crosslinking mechanism is not known, it

is expected to involve transesterification with the secondary alcohol of glycerol. This resulted in increased gel content due to addition of nanosilicates.

The addition of nanosilicates was expected to increase the swelling ratio of PGS networks as nanosilicates are hydrophilic. The swelling ratios for PGS nanocomposites containing 0%, 1%, 5%, 10%, and 15% nanosilicates were 0.99 ± 0.04, 1.02 ± 0.04, 1.04 ± 0.01, 1.05 ± 0.02, and 1.05 ± 0.03, respectively (figure II.2b). Additionally, the contact angles of a water droplet on nanocomposites decreased with increasing nanosilicates contents (figure II.2c). For example, the PGS surface had a water contact angle of 73.9 ± 5.2°, similar to previously reported literature.[36] The addition of 15% nanosilicates lowered the contact angle to 59.7 ± 1.5°, indicating increased in hydrophilicity of nanocomposites. The increase in hydrophilicity was likely due to the polyions present on the nanosilicate surfaces that attracted water molecules and thus, swelling ratio. These properties would affect degradation kinetics as well as cellular responses to the nanocomposites as water molecules at the interfaces influenced protein adsorption and cell adhesion.

To evaluate the effect of nanosilicate on surface properties of nanocomposite, protein adsorption on surface was investigated (figure II.2d). Proteins adsorbed on the surfaces could affect cell attachment and growth. We soaked the samples in Dulbecco's phosphate buffered saline (DPBS) containing 10% fetal bovine serum (FBS). The result indicated that the protein adsorbed on PGS and PGS-nanosilicates were two-fold more than that tissue culture polystyrene control. Whereas the addition of nanosilicates to PGS had no statistically significant effects on protein adsorption compared to PGS.

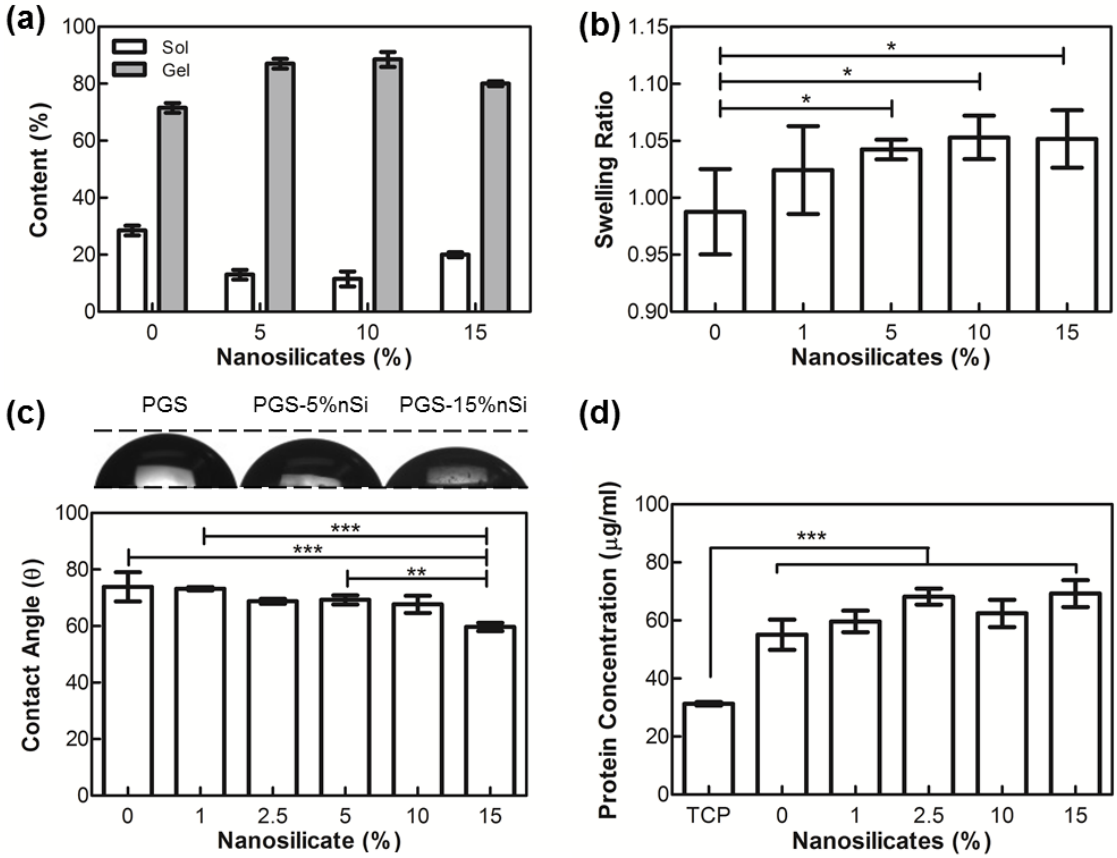

Figure II.2 Effects of nanosilicates on crosslinking density and hydrophilicity. (a) Soluble contents of PGS and PGS-silicates nanocomposites were determined via sol-gel content. Since nanosilicates also acted as crosslinkers, sol fraction decreased upon the addition of nanosilicates. Increases in nanosilicate contents also resulted in (b) higher swelling ratio in physiological conditions and (c) decreased contact angle. (d) However, the addition of nanosilicates had no effects on protein adsorption compared to PGS (statistical significance was shown as *$p < 0.05$, **$p < 0.01$, ***$p < 0.001$).

II.3.2 Nanosilicates Improved Physiological Stability of Nanocomposites

Degradation properties of biomaterials have profound effects on their applications in tissue engineering, where scaffolds need to provide structural support while degrading in the rate that matches the rate of new tissue regeneration. Under physiological conditions, PGS degrades by surface erosion *via* cleavage of ester bonds. This is advantageous over bulk-degrading polymers, since PGS exhibits gradual loss in mechanical strength and geometry, in relation to mass loss.[33] After 4 weeks in PBS, the samples were imaged using scanning electron microscope (SEM) to examine the effect of degradation on surface morphology. The images showed that the nanocomposite with higher nanosilicate content underwent significantly less degradation (figure II.3a). Specifically, for PGS and PGS-1% nanosilicates, a great extent of surface erosion and agglomeration of degraded products were observed. On the other hand, the changes in surface morphology of PGS-10% nanosilicates were minimal. The samples were intact and maintained their disk shape over the 4-week period. This, together with SEM images, indicated surface eroding nature of the nanocomposites. This characteristic is beneficial for tissue engineering application as the scaffolds will be able to maintain structural integrity in relation to mass loss during new bone regeneration.

Degradation profiles of PGS and PGS-nanosilicates nanocomposites were investigated under physiological conditions (PBS, 37°c) for 4 weeks. From the results, it was apparent that percentage of weight loss significantly reduced with increasing nanosilicate concentrations. For example, on day 10, the weight losses for the samples containing 0%, 5%, 10%, and 15%, were 25 ± 3%, 23 ± 1%, 17.5 ± 2%, and 9.8 ±1.2%, respectively (figure II.3b). Statistical analysis revealed significant differences of weight loss upon the addition of nanosilicates for all studied time points (i.e., day 3, 7, and 10). . These results indicated that the addition of silicates retard the degradation of the polyester backbone and enhance physiological stability by increasing the degree of crosslinking.

It has been reported that nanosilicates disintegrated slowly at pH < 9, while PGS underwent hydrolysis of ester groups and released carboxylic groups. The short-term degradation of PGS and PGS-nanosilcates were mainly dominated by hydrolysis of PGS. A long-term degradation profile involving disintegration of nanosilicates over a period of months will need to be evaluated in the future. Nevertheless, it should be noted that degradation of PGS *in vivo* was reported to be faster than *in vitro.*[36] *In vivo* degradation of PGS was accelerated by esterases present in the surrounding microenvironment.

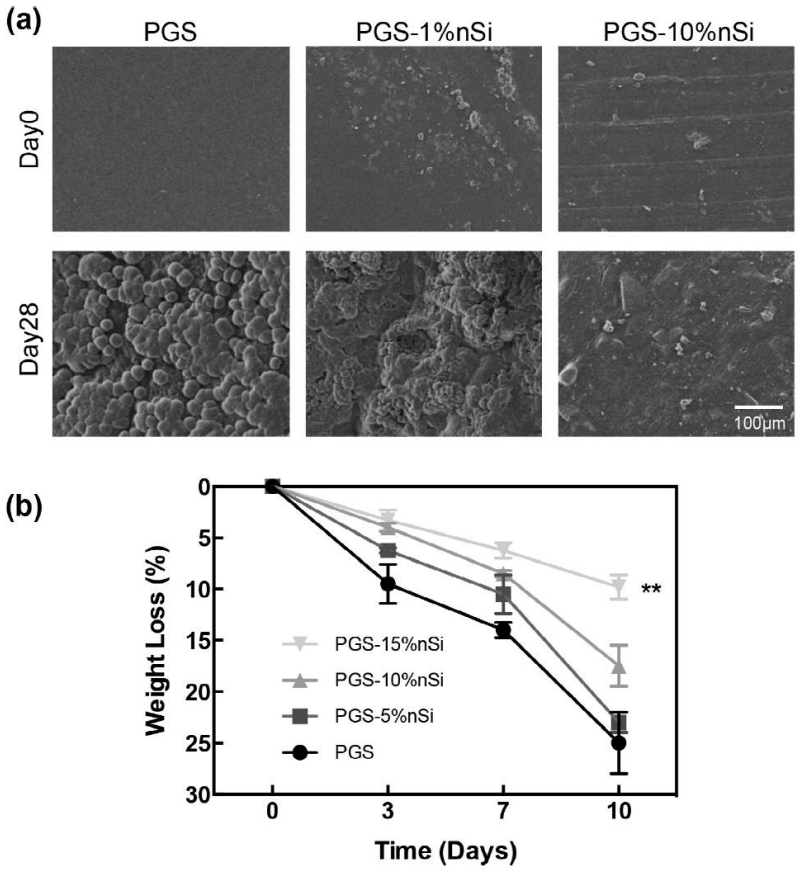

Figure II.3 Effects of nanosilicates on degradation. The addition of nanosilicates to PGS increased the stability of nanomcomposites in physilogical conditions. (a) For PGS and PGS-1%nanosilicates, agglomerated polymer degradation products were observed all over the surface after 28 days. The nanocomposites with 10% nanosilicate underwent significantly less surface errosion compared to PGS. (b) Percentage of weight loss in PBS decreased with increasing nanosilicate content. Nanocomposites with 15% nSi showed significant lower weight loss compared to PGS and PGS-5%nSi (**$p < 0.01$)

II.3.3 Nanosilicates Enhanced Thermal Stability of Nanocomposites

The thermal characteristics of PGS and PGS-nanosilicates nanocomposites were examined using thermogravimetric analysis (TGA). The samples were heated from 0 to 750 °C with the heating rate of 10°C min^{-1}. The addition of nanosilicates to PGS network enhanced thermal stability. The remaining weight at 750 °C increased upon the addition of nanosilicates, indicating higher thermal stability (figure II.4a). For example, pure PGS was completely decomposed at 750 °C, while PGS-15% nanosilicates had 7.2 ± 1.3% weight remained. The first derivative of TGA curves revealed 2-phase thermal degradation profiles (figure II.4b). The first degradation phase corresponded to the decomposition of crosslinked PGS, at which the temperature was comparable amongst all compositions (approximately 450°C). The second phase corresponded to a decomposition of crosslinked nanosilicate-PGS networks. The decomposition temperature corresponding to the second phase of thermal decomposition increased with increasing nanosilicate contents. In other words, it took longer time and higher temperature to thermally decompose the crosslinked regions of nanocomposites containing nanosilicates. The results suggested that nanosilicates enhanced thermal stability of the nanocomposites owing to increased degree of crosslinking.

II.3.4 Nanosilicates Enhanced Mechanical Stiffness of Nanocomposites

We aimed to use PGS-nanosilicate nanocomposites for bone regeneration at load bearing sites where they need to withstand repetitive compressive loadings. PGS is an elastomeric polymer and extensively investigated for soft tissue engineering applications.[33] For bone tissue engineering application, the strength and toughness need to be enhanced, ideally to match those of cancellous bone. In addition to osteoinductive properties, nanosilicates has been demonstrated to drastically improve mechanical properties of soft nanocomposite materials.[27, 36] So we expect that the addition of nanosilicate to PGS will enhance the mechanical stiffness of nanocomposite network.

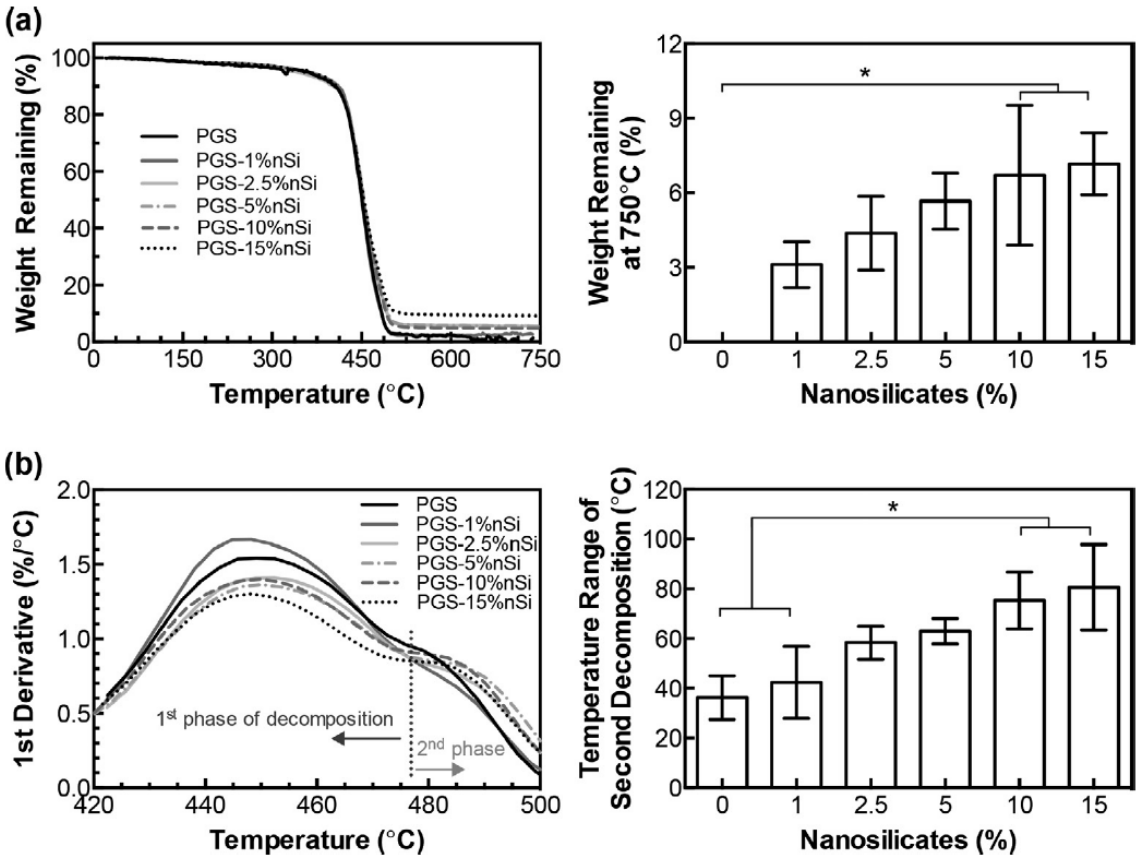

Figure II.4 Effects of nanosilicates on thermal properties. (a) Thermogravimetric analysis indicated the addition of nanosilicates significantly enhanced thermal stability of the networks. (b) The first derivative of the thermograph showed two phases of thermal decomposition. The first phase corresponded to decomposition of the crosslinked PGS network. The temperature range of the second phase, which corresponded to decomposition of PGS-nanosilicate crosslinked networks, increased with increasing silicate content (statistical significance was shown as *$p < 0.05$).

To evaluate the elastomeric properties, PGS and PGS-nanosilicate nanocomposites were subjected to 5 cycles of cyclic compression until 20% strain (figure II.5a). PGS exhibited non-linear stress-strain curve, which is a characteristic of soft elastomeric biomaterials. The stress-strain curve was used to determine the modulus of the crosslinked networks. The compressive modulus of nanocomposite was increased with increasing nanosilicate concentration (figure II.5b). The modulus was found to be 1.67 ± 1.15 MPa for PGS, which is comparable to literature. The addition of 1%, 2.5%, 5%, and 15% nanosilicates

to PGS resulted in 1.93 ± 0.89 MPa, 3.22 ± 0.51 MPa, 6.61 ± 0.27 MPa, and 8.39 ± 0.30 MPa, respectively. The addition of 15% nanosilicates engendered 5-fold increase in compressive modulus. Such enhancements could be attributed to strong interactions between nanosilicate and PGS which restricted movement of polymer chains during deformation and improved load-transfer efficiency within the network.

Energy absorbed by the network during each cycle, and percentage recovery, were also determined (figure II.5c). The maximum energy was absorbed during the first cycle. For subsequent cycles (2-5 cycles), energy absorption was relatively constant for the network. Pure PGS absorbed 5.9 ± 4.4 kJ/m^3 during the first cycle and approximately 2.1 ± 1.6 kJ/m^3 during cycle 2-5. The addition of nanosilicates significantly increased energy absorption, indicating enhanced toughness. For example, during the first cycle nanocomposites containing 1% and 15% nanosilicates exhibited energy absorption of 29.3 ± 5.9 kJ/m^3 and 65.7 ± 3.6 kJ/m^3, respectively. In comparison to PGS, over 11-fold increase in toughness was observed due to the addition of 15% nanosilicates.

Network recovery (%) upon reloading was calculated from the stress-strain curves (figure II.5d). A crosslinked network of PGS is composed of covalently-linked random coils with hydroxyl groups attached to their backbone. Covalent crosslinks and hydrogen bonds between hydroxyl groups contributed to its elastomericity.[33, 36] Interestingly, the addition of nanosilicates resulted in significantly improved mechanical strength and toughness without compromising elastomeric properties of PGS. There was no statistically significant difference between elastic recovery of all PGS and PGS-nanosilicate compositions. For example, the percentage of recovery upon reloading of nanocomposites containing 0%, 5%, and 15% nanosilicates was found to be 85.6 ± 13.6%, 91.9 ± 4.4%, and 93.1 ± 2.0%, respectively. Overall, the addition of nanosilicates to PGS has been shown to enhance energy absorption by 11-fold, increase compressive modulus by 5-fold, while maintaining elastomeric properties of the polymer. These properties of PGS-nanosilicate nanocomposites are promising for bone regeneration application.

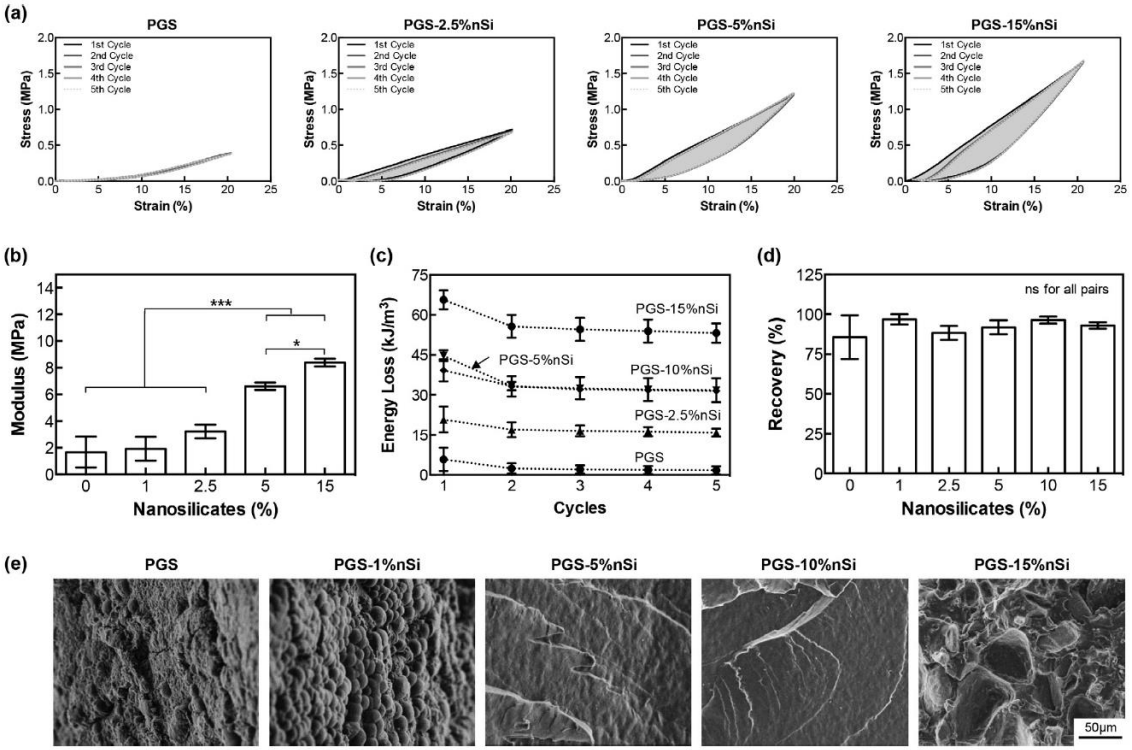

Figure II.5 Effects of nanosilicates on mechanical properties. (a) Cyclic compression of PGS and PGS-nanosilicates nanocomposites. (b) More than 4-fold increase in compressive modulus was observed due to the addition of 10% nanosilicates. (c) Also, nanosilicates enhanced toughness of the networks. The energy absorbed was maximum during the first cycle, and stayed relatively constant in the subsequent cycles. (d) With increased compressive strength, PGS-nanosilicates were able to maintain elastomeric properties, i.e., nanosilicates had no significant effects on % recovery upon reloading. (e) Electron micrographs of fractured surfaces showed ductile fracture of elastomeric PGS, and more brittle-like fractures upon the addition of silicates (statistical significance was shown as *$p < 0.05$, ***$p < 0.001$).

As PGS nanocomposite were highly elastomeric, we were not able to observed any fracture until high deformation. In order to complement the cyclic compression tests, we examined the fracture mode of PGS and PGS-nanosilicate composites by subjecting them to a uniaxial tension until break. The fractured surfaces were imaged using scanning electron microscope (SEM) (figure II. 5e). The fractured surface of PGS and PGS-1%nanosilicates showed the forming of stress concentration that eventually led to failure. The surfaces appeared rough and irregular, consisting of microvoids and dimples. These are typical characteristics of ductile fractures where the crack propagates

slowly and is accompany by large amount of plastic deformation. PGS nanocomposites with 5% and 10% nanosilicates had smoother fractured surfaces, indicating a shift toward brittle fracture. The fractured surface of PGS-15%nanosilicates displayed a mixture of transgranular and intergranular fractures, which are typically observed in a brittle fracture. Nevertheless, the nanocomposites were able to withstand repetitive loading with almost complete recovery and the surface fractured only after extensive tensile strain ~ 300%, which is not observed in physiological conditions. So, we did not investigate the tensile characteristics of nanocomposites.

II.3.5 Nanosilicates Enhanced *In vitro* Bioactivity

The bone-bonding ability of materials can be evaluated by the ability of hydroxycarbonate apatite (HCA) layer to form on its surface in simulated body fluid (SBF) (figure II.6a).[42] HCA is similar to the natural bone mineral, calcium-deficient hydroxyapatite (CDHAp), and is thought to be involved in interaction with collagen fibrils, protein adsorption, and bone progenitor cells' attachment and differentiation.[9] FTIR spectra of PGS submerged in 10X SBF for 6 hours contained two weak vibrational bands at 571 and 602 cm^{-1}, which corresponded to the P-O bending of PO_4^{3-} (figure II.6b). According to the literature, this was an indication that a crystalline phase of HCA had started to develop. Intensities of these two peaks were significantly enhanced for PGS-2.5%nSi soaked in SBF. The spectra of PGS-2.5%nSi also showed a strong band at 1035cm^{-1} assigned to P-O stretching and a band at 1544 cm^{-1} assigned to C-O stretching of CO_3^{2-}. These phosphate and carbonate bands indicated the formation of a crystalline HCA layer on the nanocomposite surfaces. Comparably, the aforementioned phosphate and carbonate bands were missing in the FTIR spectrum of the PGS and PGS-nSi before submersion in SBF. In addition, the samples immersed in 10X SBF for 30 minutes were stained for calcium with Alizarin Red S (ARS) dye and quantified (figure II.6c). It was apparent that the addition of nanosilicates resulted in significantly increased mineralization. For example, more than 3-fold increase in ARS staining was resulted from the addition of 1% nanosilicates. SEM images also showed that hydroxycarbonate apatite (HCA) started to deposit on PGS and PGS-nanosilicate nanocomposites after 30-

min immersion in 10X SBF; and the HCA layer developed over time (figure II.6d). It was apparent that the deposition increased upon the addition of nanosilicate. For example, after 6 hours, the surface of PGS-2.5%nanosilicates was almost completely covered by the HCA layer. Overall, these results clearly indicated that nanosilicates could significantly enhanced biomineralization, and the PGS-nanosilicates nanocomposites are promising biomaterials for bone regeneration.

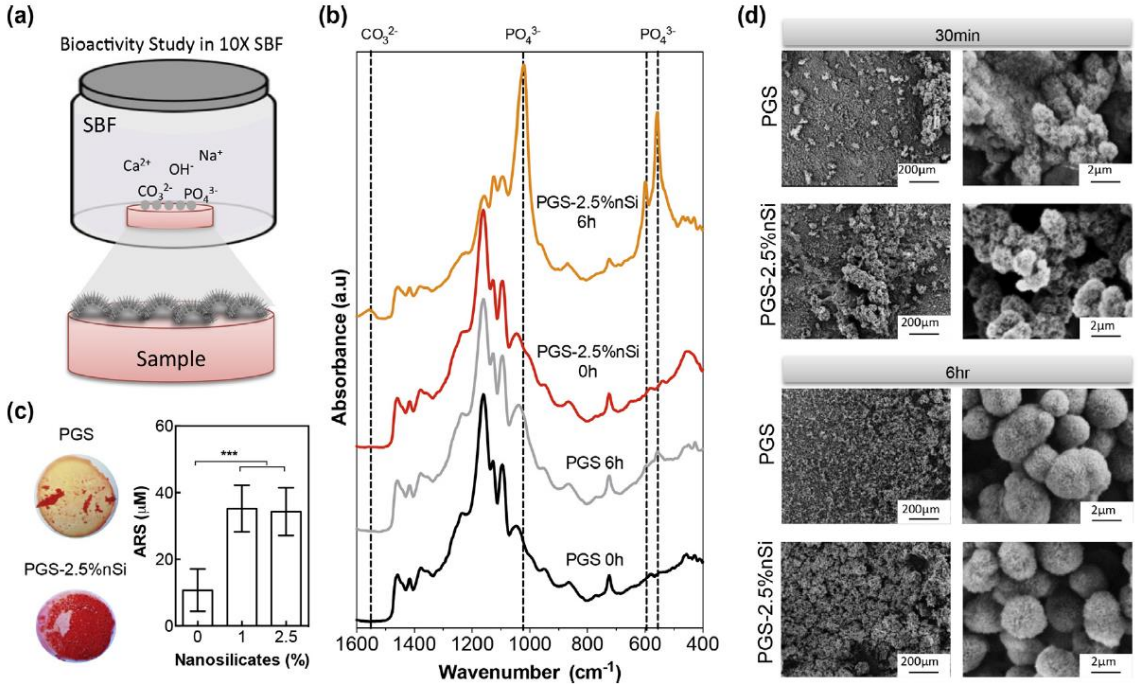

Figure II.6 In vitro bioactivity of nanocomposite. (a) The ability of nanocomposite to facilitate hydroxycarbonate apatite (HCA) on the surface was evaluated by subjecting to simulated body fluid (SBF). (b) FTIR spectra showed phosphate and carbonate bands designated to the HCA layer on PGS nanocomposites. The formation of HCA layer increased upon the addition of nanosilicates, as evidenced by (c) Alizarin Red S (ARS) staining for calcium and (d) SEM images. These results suggested that nanosilicates significantly enhanced bone bioactivity of the nanocomposites (***$p < 0.001$).

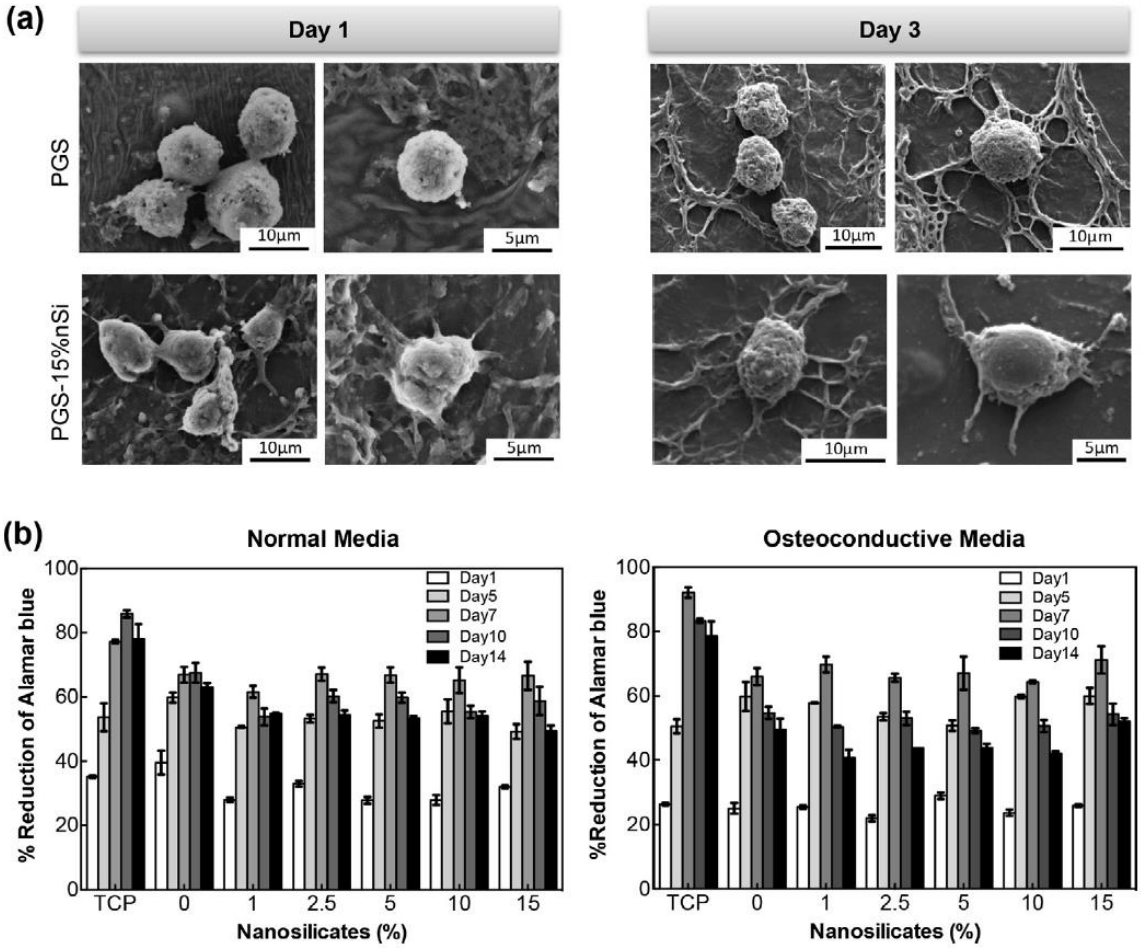

Figure II.7 Cellular adhesion and proliferation on nanocomposites. (a) PGS and PGS-nanosilicates supported initial cell adhesion. The cell spreading increased upon the addition of nanosilicates. (b) Both PGS and nanocomposite supported cell proliferation over a period of 14 days and no significant difference was observed between the groups.

II.3.6 Nanosilicates Enhanced Cell Adhesion and Proliferation

Initial cell adhesion to biomaterials surface play an important role in cell spreading, proliferation, and differentiation. The preosteoblasts cells were seeded on PGS and PGS-silicates and cell adhesion and spreading was evaluated. All substrates supported cell adhesion. Remarkably, cell spreading was enhanced with the addition of nanosilicate, whereas cells on pure PGS appeared spherical (figure II.7a). This could be attributed to higher surface stiffness or the presence of nanosilicates, or their combinatorial effects.

Our earlier reports showed that the addition of nanosilicates to non-fouling and resistance to cell adhesion surfaces (polyethylene glycol (PEG)), results in enhanced cell adhesion and spreading.[43-46] In a similar study, PNIPAM hydrogels did not support adhesion of fibroblasts and endothelial cells, however, the addition of nanosilicates support cell adhesion in a concentration-dependent manner.[47] It was proposed that nanosilicates provide cell adhesion sites for protein adsorption that subsequently facilitate cell adhesion, however, the actual mechanisms are still unclear.

Proliferation of cells seeded on PGS and PGS-silicates were investigated by analyzing their metabolic activity over two weeks using alamarBlue® assay. All nanocomposite surface supported proliferation of preosteoblasts (figure II.7b). The metabolic activities of cells increased with time and started to decrease after 1 week of culture. This could be attributed to the cells reaching confluency. Cell proliferation in osteoconductive media was slightly higher than that in normal growth media; however, there was no statistical difference between the groups. In addition, no significant difference in the metabolic activities was observed due to the addition of nanosilicates. This was opposite to the previous reports that the addition of nanosilicates to PEO resulted in increased metabolic activity in a concentration-dependent manner.[44] This discrepancy could be explained by the fact that PEO exhibited low cell attachment, thus, significant enhancement was observed upon the addition of nanosilicates. On the other hand, PGS itself is cell adhesive, and has been demonstrated in the literature to be cytocompatible and support cell proliferation. From the metabolic activity study, it was evidenced that cell proliferation on PGS and PGS-nanosilicates were higher than that on TCP during the first week and vice versa in the second week, unlike the PEO-nanosilicates system in which cell proliferation on the nanocomposites with 70% nanosilicates was still significantly lower than that on TCP.

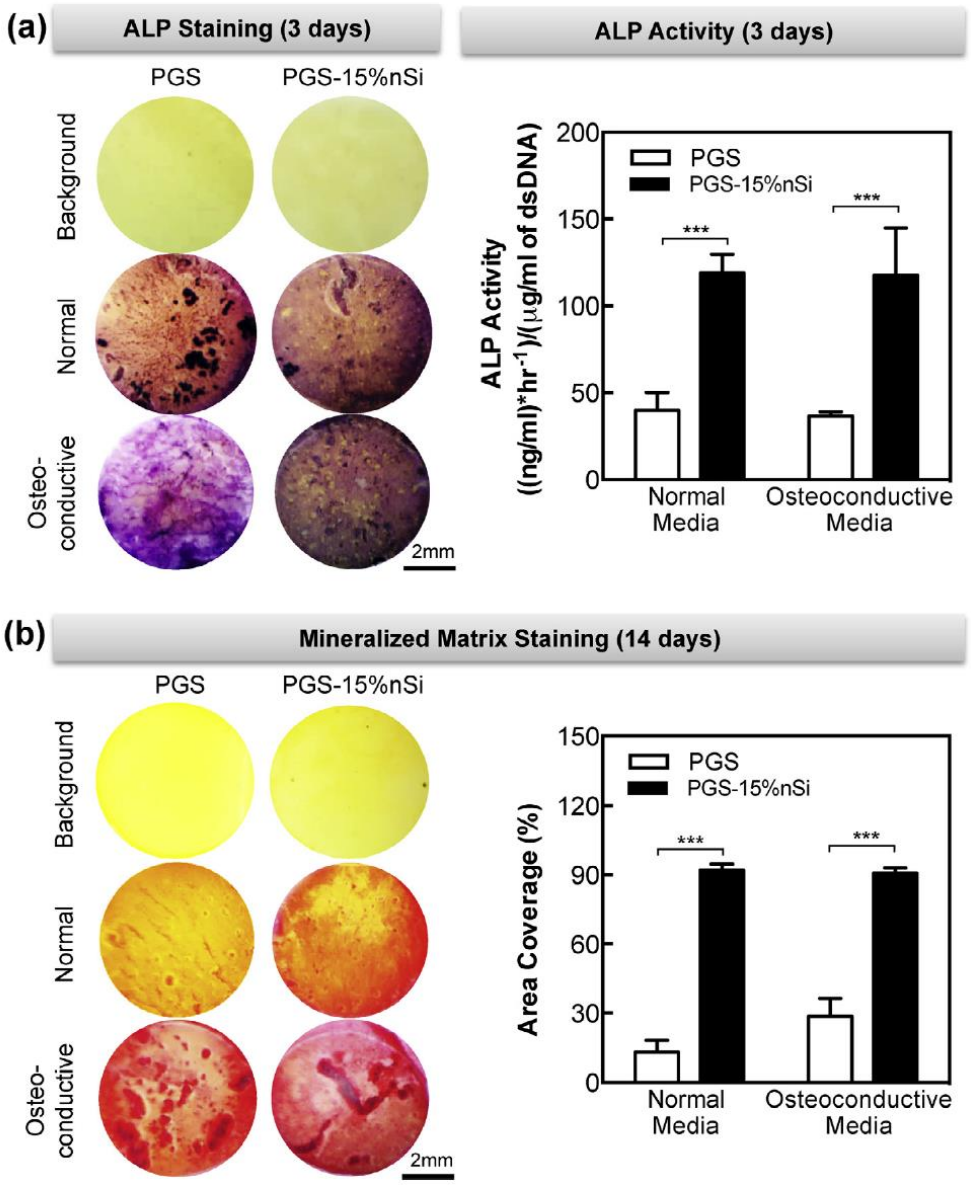

Figure II.8 Differentiation of preosteoblasts on PGS nanocomposites. The addition of nanosilicates enhanced osteogenic differentiation of seeded cells as evidenced by (a) increased alkaline phosphatase (ALP) activity on day 3 and (b) increased matrix mineralization on day 14. The images of stained samples were quantified and plotted (right figures). Also, it should be note that matrix mineralization in osteoconductive media was significantly higher than that in normal media (***$p < 0.001$).

II.3.7 Differentiation of Preosteoblasts on PGS and PGS-nSi

The ability of PGS-nanosilicate nanocomposites to promote osteogenesis was determined by assessment of ALP and matrix mineralization production by the seeded cells in both normal growth and osteoconductive media (αMEM supplemented with β-glycerophosphate and ascorbic acid). As an early marker of osteogenic differentiation, ALP staining and subsequent image quantification was performed on day 3. In both media conditions, PGS-nSi nanocomposites displayed stronger ALP staining compared to PGS (figure II.8a). The quantification of ALP activity further confirmed the results. There was no apparent difference in the staining between the normal growth and the osteoconductive groups at this time point. The increases in ALP activity with the addition of nanosilicates indicated a key role of nanosilicates in upregulating osteogenic differentiation.

Furthermore, matrix mineralization is a late-stage marker of osteogenic differentiation, was assessed on day 14 by ARS staining. The addition of nanosilicates resulted in significant increases in ARS staining in a concentration-dependent manner (figure II.8b). Moreover, the samples in osteoconductive media displayed higher ARS staining compared to the cells seeded in normal growth media. Image quantification showed more than 2-fold increase in percentage of area coverage upon the addition of 15% nanosilicates when cultured in growth media. It is important to note that the enhancement of both ALP activity and matrix mineralization with increasing nanosilicate concentrations were observed in the absence of osteogenic factors such as bone morphogenic protein 2 (BMP2) and dexamethasone. In particular, nanosilicates promoted ALP and mineralized matrix deposition even when the preosteoblasts were cultured in normal growth media. In a summary, the results indicated that nanosilicates could promote osteogenic differentiation of preosteoblasts without any osteogenic factors. These agreed with previous works reporting osteoinductive properties of nanosilicates.[15, 48]

II.4 SUMMARY

We successfully fabricated PGS-nanosilicates elastomeric nanocomposites. Degree of crosslinking, hydrophilicity, thermal and structural stability can be tailored by addition of nanosilicate. Importantly, mechanical strength and stiffness could be enhanced while the elastomeric property of the polymer was still preserved. *In vitro* mineralization also showed increased bioactivity upon the addition of nanosilicates. The nanocomposites supported attachment and proliferation of MC-3T3 preosteoblasts and significantly promoted osteogenic differentiation of cells in the absence of osteogenic factors, suggesting osteoinductive properties of the nanocomposites. Overall, these indicate that PGS-nanosilicate nanocomposites can be used for bone tissue engineering applications.

CHAPTER III

MANUSCRIPT#2: ELASTOMERIC POLY(GLYCEROL SEBACATE)/NANOSILICATES SCAFFOLDS: A GROWTH-FACTOR-FREE APPROACH FOR BONE TISSUE ENGINEERING

III.1 OVERVIEW

Bone is the second most transplanted organ following blood, and significant advanced have been made in developing synthetic bone graft substitutes and scaffolds. However, there remains a critical need for osteoinductive scaffolds with mechanical functionality for bone tissue engineering at load-bearing sites. Here, we reported nanocomposite scaffolds of elastomeric poly(glycerol sebacate)(PGS) and osteoindictive nanosilicates, fabricated via salt-leaching method. The addition of nanosilicates to PGS matrix resulted in enhanced physical integrity as well as increased mechanical strength and toughness. Remarkably, elastomeric properties of the scaffolds were not compromise, providing a load-transducing environment for bone regeneration. PGS/nanosilicates scaffolds supported cell proliferation and promoted cell spreading. The addition of nanosilicates upregulated osteogenic differentiation of seeded preosteoblasts in a concentration-dependent manner as evidenced by increased ALP activity and matrix mineralization, even when cultured in normal growth media without any osteogenic factors. All in all, the combination of elasticity and tunable stiffness, tailorable degradation profiles, and the ability to promote osteogenic differentiation of the scaffolds offered a promising growth-factor-free approach for bone tissue engineering.

III.2 MATERIALS AND METHODS

III.2.1 Poly(glycerol sebacate)(PGS) Synthesis

Poly(glycerol sebacate)(PGS) was synthesized via polycondensation of glycerol and sebacic acid in 1:1 molar ratio according to previously published procedures. Glycerol ($C_3H_8O_3$) and sebacic acid ($C_{10}H_{18}O_4$) were used as purchased (Sigma-Aldrich). Briefly, equimolar glycerol and sebacic acid were mixed in a two-neck round-bottom flask, and heated to 120°C under nitrogen gas for 24 hours. Then, the pressure was gradually reduced to 50mTorr, and the reaction was continued for 48 more hours. After the reaction was finished, the vacuum was turned off, filling the flask with Argon gas. The prepolycondensed polymer (polymer) was cooled down to room temperature then kept in 4°C refrigerator for future use. Polycondensation reaction of PGS synthesis and schematic of PGS/nanosilicates crosslinked networks were illustrated in figure III.1.

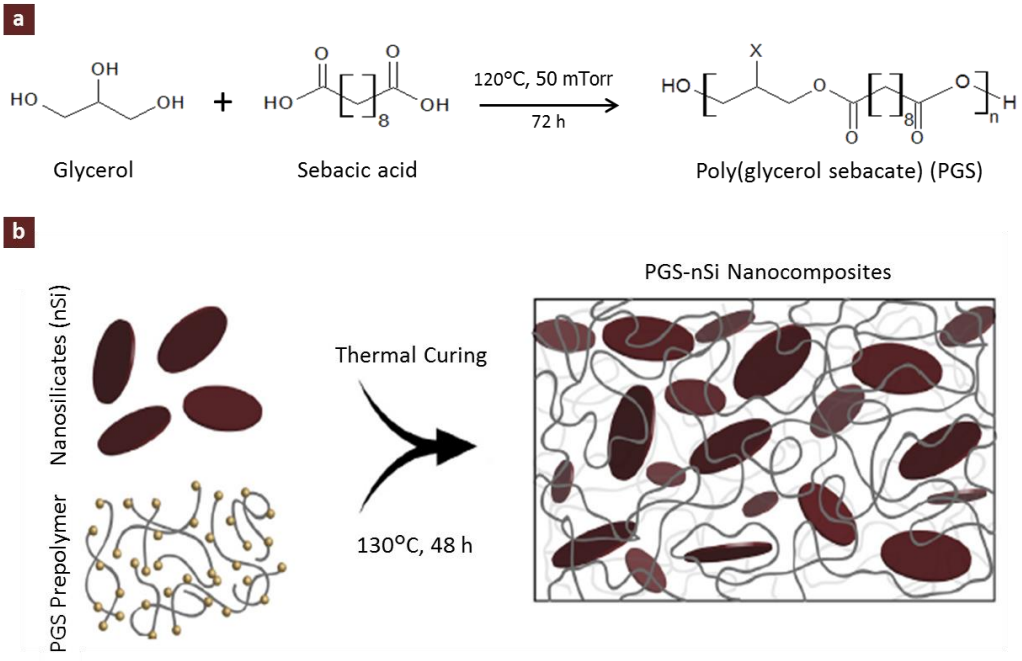

Figure III.1 PGS synthesis and PGS/nanosilicates nteworks. (a) PGS was made from polycondensation reaction between glycerol and sebacic acid under vacuum at 130°c and 50mTorr for 72h. (b) PGS and silicate nanoplatelets were mixed in 30%ethanol-70%chloroform. Thermal curing at 130°c for 48hr yielded the fully crosslinked networks.

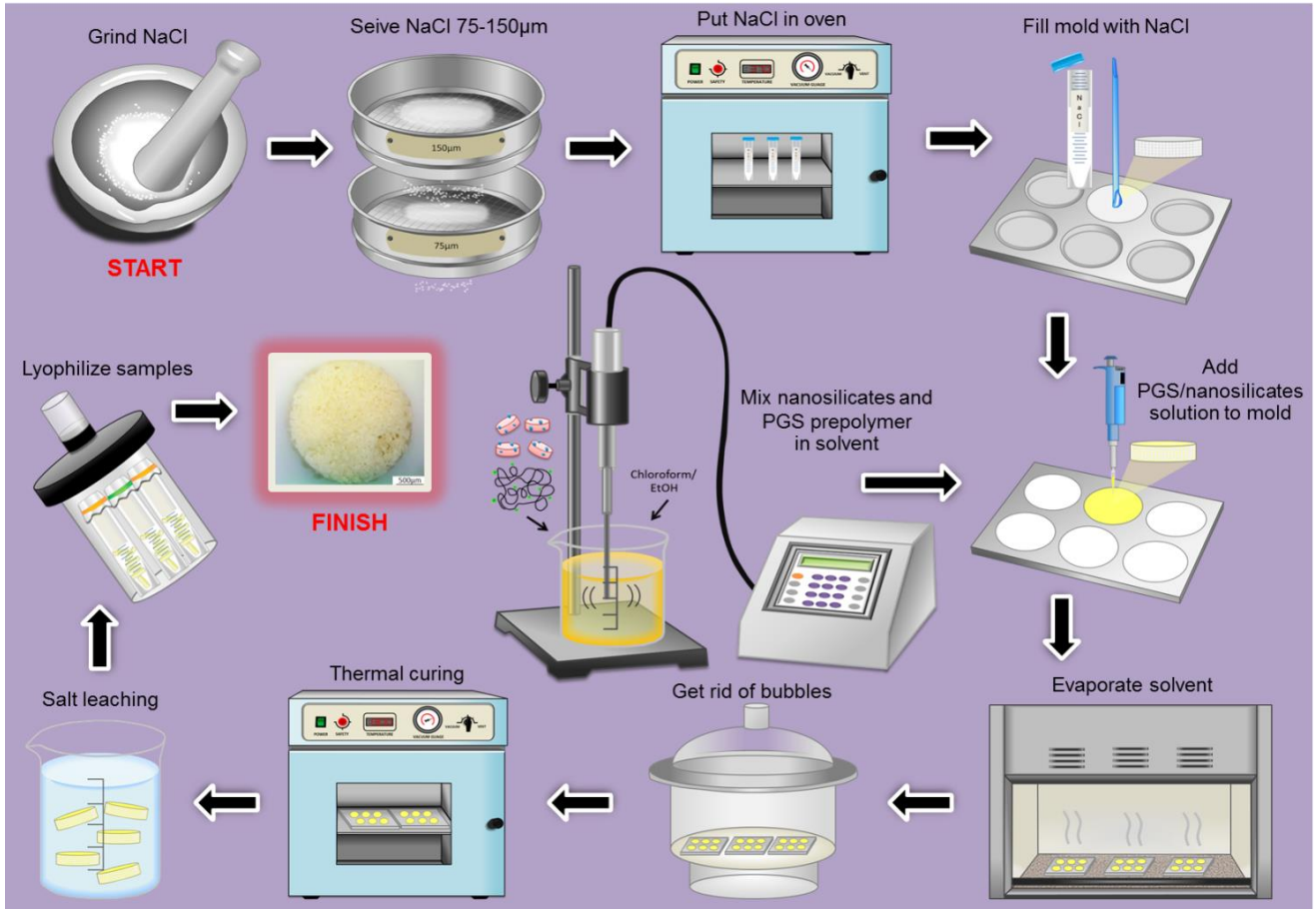

Figure III.2 Porous scaffolds fabrication procedures. PGS/nanosilicates scaffolds were fabricated via salt leaching technique. Briefly, NaCl with the size between 75µm and 150µm was used as porogen. Nanosilicates and PGS prepolymer were mixed in chloroform/ethanol solvent using a probe sonicator. Then, the solution was added to salt-filled teflon molds. The samples were left in a fume hood for solvent evaporation, then put in a vacuum dessicator for further air bubble elimination. Thermal curing at 130°C for 48hr yielded fully crosslinked PGS/nanosilicates networks. Individual samples were then removed from the molds and submerged in deionized water with agitation for salt leaching. The leached salts left empty space behind which created pores. Lastly, the porous samples were lyophilized, and the dried porous nanocomposite scaffolds were ready for further studies.

III.2.2 Fabrication of PGS and PGS-Nanosilicate (PGS-nSi) Scaffolds

Porous scaffolds were fabricated by salt-leaching method. Briefly, NaCl (Sigma-Aldrich, ACS reagent grade) was grinded using a mortar and pestle, and then sieved to gather crystals that fall between 75 and 150μm diameter to use as porogens. VWR sieves #100 (150μm opening) and #200 (75μm opening) were used. Teflon molds were completely filled with sieved salts, and put into an oven overnight at 37°C. The teflon molds were custom made to have a size of 6mm diameter and 2mm thickness. Next, in a glass vial, mix PGS pre-polymer in 70% chloroform-30% ethanol (50%w/v), then add 0%, 1%, 2.5%, 5%, and 10% of nanosilicates. A probe sonicator (Model FB120, Fisher Scientific) was used to disperse nanosilicates in PGS pre-polymer solution until it turned homogeneous. The solution was added to the molds over the salt; allowed it to penetrate between salt crystals until all the spaces were filled. The samples were left in a fume hood for 48 hours for solvent evaporation, then another 24 hours in a vacuum dessicator for air bubble elimination. Fully crosslinked networks will be achieved by thermal curing in a vacuum oven at 130°C for 48 hours. Then, the crosslinked samples were removed from the molds, and submerged in deionized water under agitation to leach out the salt. The salt leaching process took 36 hours, with water changing every 4 hours for the first 12 hours. The scaffolds were lyophilized, and stored in a vacuum dessicator until further studies. The fabrication procedures are illustrated in figure III.2. The scaffolds were named PGS, PGS-1%nSi, PGS-2.5%nSi, PGS-5%nSi, and PGS-10%nSi, according to nanosilicate concentration.

III.2.3 Surface and Cross-section Morphology

After successfully fabricated, surface and cross-section images of the scaffolds were taken using a scanning electron microscopy (SEM) (Neoscope JCM-5000). For cross-section imaging, the scaffolds were broken into half while submerged in liquid nitrogen in order to preserve their porous structure. The samples were dried in a vacuum dessicator, then sputter coated with Au/Pd before mounted onto specimen stubs with a carbon tape.

III.2.4 Degradation Studies

Scaffolds were submersed in 0.01M NaOH over 1-week period at 37°C. After 1, 2, 4, 7 days, the samples were collected, lyophilized, and dried weight was measured. Percentage of weight loss at each time point was calculated from the initial (W_i) and final (W_d) dried weight using equation III.1.

$$\text{Weight loss (\%)} = \frac{W_i - W_d}{W_i} x100 \qquad \text{(Equation III.1)}$$

III.2.5 Mechanical Properties

Scaffolds were subjected to 8 cycles of cyclic compression (eXpert 7600, ADMET, USA) with the strain rate of 0.1mm/min until 60% strain. Stress-strain curves, compressive modulus, energy dissipation, and percentage of recovery upon reloading were determined.

III.2.6 Protein Adsorption

Fetal bovine serum (FBS) protein was used for protein adsorption study. Scaffolds were washed twice with Dulbecco's phosphate buffered saline (DPBS) before soaked in 10% FBS in an incubator at 37°C, 5% CO_2, for 24 hours. DPBS and FBS were purchased from Life Technologies. After 24 hours, FBS was removed, and the samples were gently washed with DPBS trice to remove non-specifically adsorbed proteins. Then, 2% sodium dodecyl sulfate (SDS) solution was added, and the well plate was shaken for 6 hours to collect adsorbed proteins. SDS solution (20%) purchased from Amresco was diluted by DPBS to make 2% SDS solution used in the study. Protein concentration in the collected solution was quantified using a Micro BCA™ Protein Assay Kit (Thermo Scientific) following manufacturer's protocols. Briefly, an equal amount of collected protein solution and BCA working reagent were incubated at 37°C for 2 hours then the UV absorbance was read using a UV/Vis spectrophotometer (Infinite M200PRO, TECAN) at 562 nm. Bovine serum albumin (BSA) came with the BCA assay kit was used a standard for absorbance-concentration conversion.

III.2.7 Cell Culture and *In vitro* Cell Adhesion

MC-3T3 E1 subclone4 preosteoblasts (ATCC®) were cultured in normal growth media (α-MEM) (Hyclone^{TM}) containing 10% FBS and 1% penicillin/streptomycin (gibco® by Life Technologies), in an incubator at 37°C and 5% CO_2 level (humidified atmosphere). The cells were used for studies at 70% confluency in culture. Before cell seeding, scaffolds were washed twice with DPBS, sterilized under UV light in a biosafety cabinet for 4 hours, then incubated in a normal growth media overnight in an incubator at 37°C. It should be noted that for all cell studies, cell-seeded scaffolds were cultured in non-treated well plates to minimize cell adhesion to the well plate (i.e. maximize cell adhesion to the samples); whereas cells seeded on treated well plates (referred to as tissue culture plate or TCP here) were used as positive controls, and non-seeded TCP as negative controls.

For cell adhesion study, the cells were trypsinized (0.5% trypsin-EDTA, gibco® by Life Technologies), centrifuged, and seeded on the scaffolds at the density of 5,000 cells/100µl media per sample per well. For initial cell seeding, the cells were cultured in normal growth media. Later, the samples were divided into 2 groups; the first group was cultured in normal growth media while the second group in osteoconductive media (α-MEM supplemented with 10mM β-glycerophosphate and 0.05mM ascorbic acid). β-glycerophosphate and ascorbic acid were used as purchased from Sigma-Aldrich. Osteoconductive media was added to the second group of samples at 24 hours after initial seeding. Cell culture media was changed every 3 days. The samples were collected after 7 days in culture and prepared for imaging. They were washed trice with DPBS, fixed with 2.5% glutaraldehyde (2.5% aqueous solution, Alfa Aesar®), and dehydrated with graded ethanol (30%, 50%, 75%, 95%, and 100%, in order). The dehydrated samples were subjected to chemical drying with hexamethyldisilazane (HDMS) (electronic grade, Alfa Aesar®) before mounted to the stub, sputter coated, and imaged with SEM.

III.2.8 In vitro Cell Proliferation and Differentiation

As mentioned previously, MC-3T3 E1 preosteoblasts were trypsinized at 70% confluency in culture, and seeded on pre-treated scaffolds at the density of 5,000cells/100µ media. Cell proliferation was assessed by determining metabolic activity using alamarBlue® assay (Thermo Scientific) following the standard manufacturer's protocol. The proliferation data was collected on day 1, 3, 5, 7, 10, 14 after the initial cell seeding. Osteogenic differentiation of seeded preosteoblasts was assessed by determining alkaline phosphatase (ALP) activity and matrix mineralization. Specifically, on day 7, the samples were stained with BCIP/NBT solution (Thermo Scientific) for ALP, following standard manufacturer's protocols. The stained samples were imaged using a microscope. ALP activity was further quantified using SensoLyte® *p*NPP Alkaline Phosphatase Assay Kit, and normalized with the amount of double strand DNA (ds-DNA). The amount of dsDNA was quantified using PicoGreen® Assay in conjunction with Nanodrop3300 fluorospectrometer (Thermo Scientific). In addition, matrix mineralization was stained and quantified on day 14. The samples were stained with Alizarin Red S (ARS) (2% solution, pH 4.2, Electron Microscopy Science) for calcium deposit, and imaged. Quantitative analysis of ARS staining was further performed. ARS-stained samples were incubated with 10% acetic acid (Fisher Scientific) with shaking for 30 minutes; the supernatant was neutralized with 10% ammonium hydroxide (Sigma-Aldrich) before UV absorbance reading at 405nm. The absorbance was converted to ARS concentration using a predetermined standard curve.

III.2.9 Statistics

The experimental results were plotted as mean ± standard deviation (n=3-5). Statistical analysis of all quantitative data was performed by one-way analysis of variance (ANOVA) while pair-wise comparison of data was determined by Turkey's post hoc test. Statistical significance was shown as $*p < 0.05$, $**p < 0.01$, $P*** < 0.001$.

III.3 RESULTS AND DISCUSSION

III.3.1 Microstructure of PGS/Nanosilicates Scaffolds

PGS and PGS/nanosilicates scaffolds were fabricated via salt-leaching method as illustrated in figure2. The resulting scaffolds had a disk shape with 2mm thickness and 6mm diameter, and appeared porous (figure III.3a). It has been reported that dimensions of PGS scaffolds became closer to those of the molds when curing temperature increased. The scaffolds could effectively maintain their dimensions without shrinking when the curing time was 36 hours or more.[49] Here, the scaffolds were cured for 48 hours under vacuum, and minimal to none shrinkage was observed. SEM images of the surface showed interconnected pores throughout the scaffolds (figure III.3b). The pore size was between 75-150μm as designed by the size of NaCl porogens. In addition, smaller micropores with the size of approximately 5-20μm were distributed between the macropores (75-150μm). It was likely that the micropores were generated during curing process. Thermal curing of PGS involved transesterification reaction.[49] This resulted in covalent crosslinking between polymer chains that created 3D network of random coils, turning the viscous liquid into solid elastomer. The solvent and air bubbles were unlikely to be the sources of micropores. Chloroform and ethanol are both highly volatile; solvent evaporation in a fume hood for 48 hours should be decent. Also, the scaffolds were kept in a vacuum dessicator for at least 24 hours before curing, minimizing air bubbles. In addition, cross-section SEM images showed that the pores were homogenously distributed across the width and depth of the scaffolds (figure III.3c). Morphology of the surface and interior appeared to be similar (figure III.3b and III.3c).

Cross-section images of all 5 compositions were shown in figure III.3d. It could be seen that the pore size was similar amongst compositions, suggesting nanosilicate concentrations had no effects on pore size. This was expected since the pore size was mainly controlled by NaCl porogens. We could account this as an advantage of salt-leaching method in comparison to other fabrication techniques; the resultant porous

structure could be better controlled, and was tunable independently from the scaffold composition. High magnification images showed that the pore walls of PGS scaffolds were relatively smooth, and the roughness increased upon the addition of nanosilicates. The increased in surface roughness could be attributed to the presence of nanosilicates and their interaction with PGS matrix. It was hypothesized that the rough topography would enhance cell adhesion and spreading.

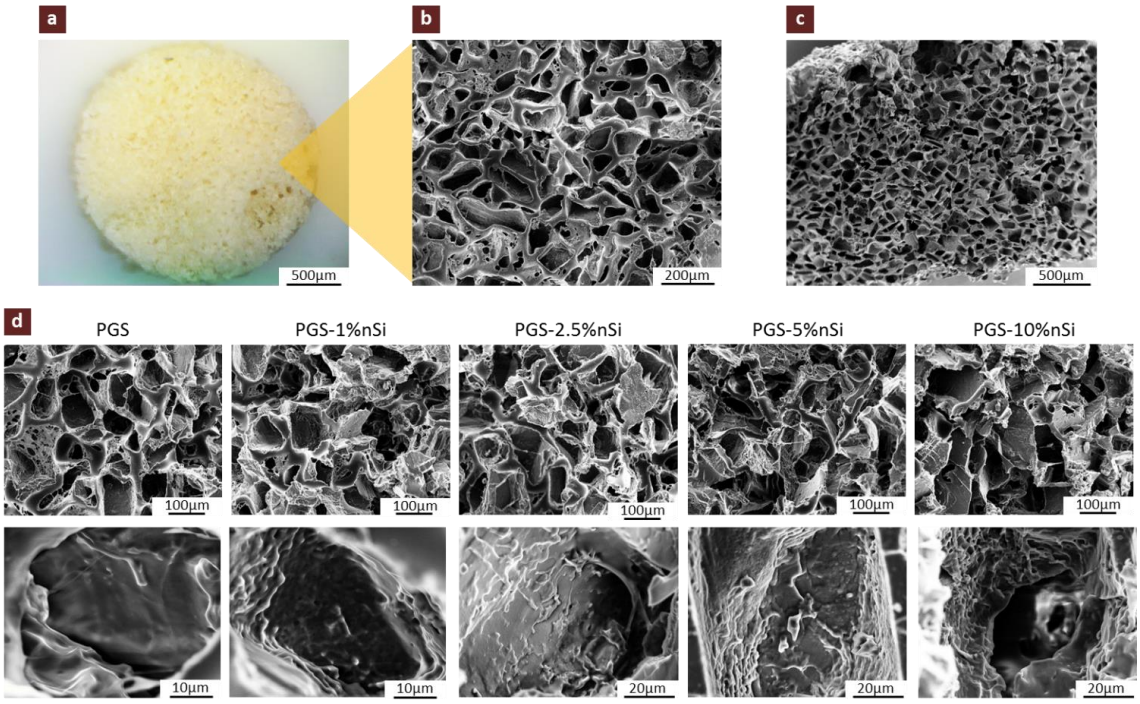

Figure III.3 PGS and PGS-nSi porous scaffolds. (a) Successfully synthesized porous scaffolds had a disk shape with 6mm diameter and 2mm thickness. Figure (b) and (c) showed SEM images of the scaffold surface (b) and cross-section (c). Morphology of the surface and interior appeared to be similar. (d) The pore size is between 75-150µm as designed by the size of NaCl porogen; and the size was similar amongst compositions. High magnification images showed that the roughness of the pore walls increased with higher nanosilicate concentration (bottom panel).

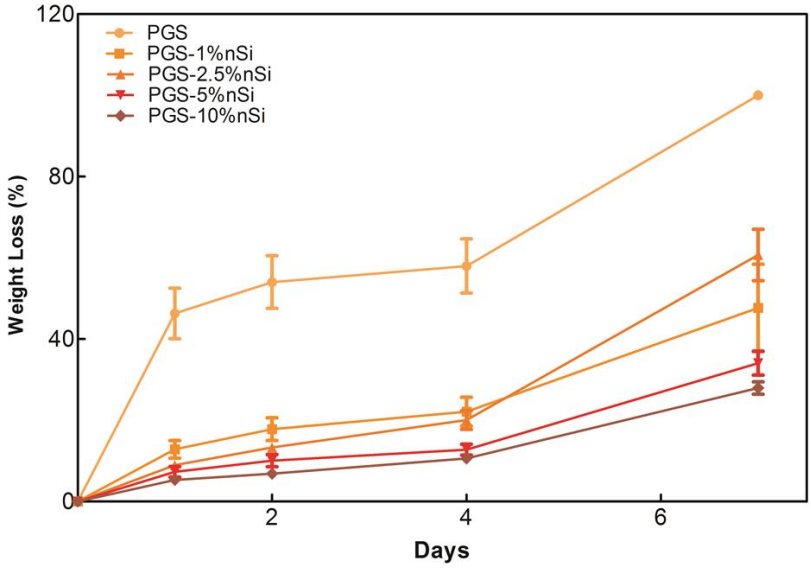

Figure III.4 Scaffold degradation in 0.01M NaOH over a week. Percentage of weight loss significantly decreased upon the addition of nanosilicates, indicating enhanced structural integrity. PGS scaffolds were degraded completely after 7 day while the addition of 10% nanosilicates resulted in more than 3.5 times decrease in weight loss. Note that the basic condition in this study accelerated the degradation process.

III.3.2 Nanosilicates Enhanced Physical Stability of the Scaffolds

It is well established that degradation profile of scaffolds has profound effects on their tissue engineering performances. Scaffolds need to provide structural support while allowing gradual replacement with newly formed bone. Under physiological condition, PGS underwent surface erosion via cleavages of ester bonds. From tissue engineering standpoint, this was preferable over bulk-degrading polymers since PGS showed gradual loss in mechanical integrity, relative to mass loss. In preliminary studies, degradation profiles of PGS and PGS/nanosilicates scaffolds were investigated under physiological conditions (PBS, 37°C) for one week. Less than 3% weight loss was observed for all samples (data now shown). With standard deviation taken into account, the differences between compositions were statistically inconclusive. Therefore, the experiment was re-conducted in 0.01M NaOH. Basic condition was used to accelerate the process, and it was anticipated that the trends would be more prominent.

Percentage of weight loss was measured on day 1, 2, 4, and 7. The results showed that weight loss significantly reduced with increasing nanosilicate concentration (figure III.4). For example, after one week, PGS scaffolds were completely degraded while PGS-10%nSi experienced only 28±3.4% weight loss. That means more than 3.5 times reduction in weight loss upon the addition of 10% nanosilicates. It should be noted here that the study was conducted in basic condition. The increases in physical integrity with the addition of nanosilicates could be observed for all studied time points. In addition, the scaffolds remained intact and maintained their shape upon degradation, i.e. they became smaller disk over time. This indicated surface eroding nature which was beneficial since the scaffolds would be able to better maintain their structural integrity during new tissue regeneration in comparison to bulk degrading scaffolds.

It has been demonstrated that degradation kinetics of PGS could be entirely tuned by varying degree of crosslinking. In this case, nanosilicates acted as crosslinkers, retarding degradation of polyester backbone resulting in enhanced physical integrity. Our previous studies showed that the addition of nanosilicates increased crosslinking density of thermally cured PGS/nanosilicates nanocomposites.[50] In that study, the degree of covalent crosslinking was determined via sol-gel content. The amount of sol content (uncrosslinked macromer) was statistically significantly reduced with increasing nanosilicate concentration. The results ascertained the role of nanosilicates as multifunctional crosslinkers as previously reported in the literature.[46, 47] It is anticipated that the crosslinking involved transesterification with the secondary alcohol of glycerol. Nevertheless, the exact mechanisms will need further investigation.

PGS degrades by hydrolysis of ester groups and releases carboxylic groups while nanosilicates slowly disintegrate at pH<9. Short-term degradation of the scaffolds was dominated by PGS hydrolysis. A complete long-term degradation profile involving disintegration of nanosilicates in physiological condition over a period of months will need to be evaluated in the future. The results shown here demonstrated the effects of nanosilicates on scaffold degradation, and that it was tailorable, but they did not

represent the actual timeframe of degradation. Also, it is important to note that PGS degradation *in vivo* was reported to be faster than *in vitro*.[43] *In vivo* degradation was accelerated by esterase present in the surrounding environment.

III.3.3 Nanosilicates Increased Mechanical Stiffness without Compromising Elastomeric Properties

Bone is a dynamic tissue to which applied loads play vital roles in determining the rate of turnover as well as the formation of callus, its volume, and stiffness during bone healing. It was reported that scaffolds possessing some elasticity provided a load-transducing environment in which osteogenesis, matrix deposition, and bone maturation could take place.[37] On the contrary, nonload-transducing scaffolds were found to have relatively inferior performance in bridging critical size bone defects. Therefore, elastomeric PGS was chosen as a base for reinforced nanocomposite scaffolds. For bone tissue engineering application, the strength and toughness of the scaffolds need to be enhanced, and that could be achieved by incorporating nanosilicates.

The scaffolds were subjected to 8 cycles of cyclic compression (figure III.5a). All samples (both PGS and PGS/nanosilicates) exhibited non-linear stress-strain curve which is a characteristic of elastomeric materials. Compressive modulus, energy dissipation, and percentage of recovery were calculated. The results showed that compressive modulus was significantly increased with increasing nanosilicate concentration, and the number was relatively constant from cycle 1 to 8 (figure III.5b). For example, from the first cycle, the compressive modulus was 27.9±5.1 kPa, 45.9±4.8 kPa, 67.2±16.1 kPa, 88.6±9.0 kPa, and 130.8±15.3 kPa, for the scaffolds containing 0%, 1%, 2.5%, 5%, and 10% nanosilicates, respectively. The addition of 10% nanosilicates engendered over 4.5 times increase in the modulus. Such enhancement could be attributed to interactions between PGS and nanosilicates which restricted movement of polymer chains during deformation as well as improved load transfer within the network. In this regard, nanosilicates have been shown to drastically improve mechanical properties of soft nanocomposites.[27, 47]

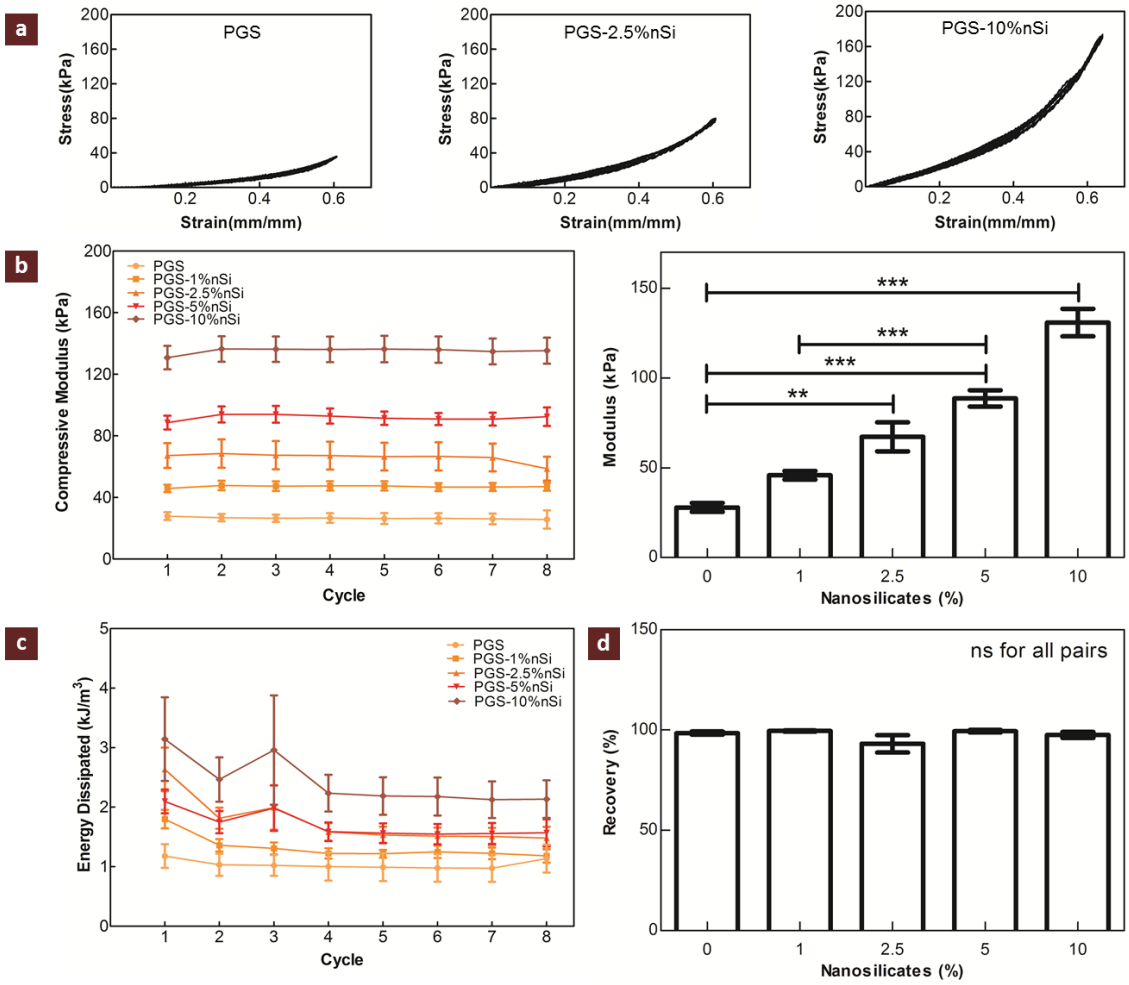

Figure III.5 Mechanical properties. PGS and PGS-nSi scaffolds were subjected to 8 cycles of cyclic compression. The first cycle was shown in figure (a). (b) The compressive modulus increased with increasing nanosilicate concentration and was comparable from cycle 1 to 8. (c) Also, energy dissipation was enhanced upon the addition of nanosilicates. The energy absorbed was maximum during the first cycle, then decreased and remained relatively constant in the subsequent cycles. Despite enhanced mechanical strength and toughness, elastomeric properties of PGS were not traded off. (d) After 8 cycles of compression, %recovery after reloading was not statistically different amongst compositions.

In addition, energy dissipation during each cycle was determined (figure III.5c). The maximum energy absorption was observed during the first cycle, then it decreased and remained relatively constant during subsequent cycles for all scaffold compositions. For example, PGS-1%nSi scaffolds absorbed 1.8±0.3 kJ/m^3 during cycle 1 and

approximately 1.3±0.2 kJ/m^3 during cycle 2-8. Moreover, energy dissipation increased with increasing nanosilicate concentrations, indicating enhanced toughness. During the first cycle, the scaffolds containing 0%, 1%, 2.5%, 5%, and 10% absorbed 1.2±0.4 kJ/m^3, 1.8±0.3 kJ/m^3, 2.6±0.8 kJ/m^3, 2.1±0.4 kJ/m^3, and 3.1±1.6 kJ/m^3, respectively. That is, the addition of 10% nanosilicates resulted in more than 2.5 times increase in toughness. Our previous studies showed that the addition of 10% nanosilicates to solid PGS/nanosilicates nanocomposites gave rise to over 6.5 times increase in energy dissipation.[50] This could be attributed to the fact that the porous structure of the scaffolds were controlled by porogens, therefore, the effects of nanosilicates was less in comparison to their nonporous counterparts.

Percentage of network recovery was also calculated from the stress-strain curves in order evaluate scaffolds' elasticity, as mentioned previously that scaffolds possessing some elasticity would provide load-transducing environment for proper bone healing. A fully crosslinked PGS network consists of covalently-linked random coils with hydroxyl groups attached to their backbone. These covalent crosslinks and hydrogen bonds between hydroxyl groups contribute to its elastomeric characteristics.[33, 36] Interestingly, the addition of nanosilicates enhanced mechanical strength and toughness without compromising elastomeric properties to the scaffolds. In particular, nanosilicate concentration did not have statistically significant effects on network recovery (figure III.5d). For example, after 8 cycles of compression, recovery of PGS and PGS-10%nSi scaffolds was found to be 98.4±1.4% and 97.6±3.4%, respectively. These results suggested that mechanical properties of PGS/nanosilicates scaffolds were tunable. The addition of nanosilicates increased mechanical strength and toughness while maintaining their elastomeric properties. This would be beneficial as there is a requirement for some flexibility in the initial phase of bone healing which involves cartilage formation before bone calcification.[51] The results suggested that the scaffolds could provide load-transducing environment for bone regeneration. As Wolff's law stated, bone will adapt to loads under which it is placed; bone will resorb if the load is not properly transduced. Too strong bone grafting materials are expected to shield the load from immature bone

leading to bone resorption/less bone volume, whereas too weak materials lead to early collapse. In the future, we aim to increase nanosilicate concentration to bring the mechanical properties closer to those of cancellous bone. Considering the achieved mechanical properties, it is promising that PGS/nanosilicates scaffolds could be used for craniofacial defects.

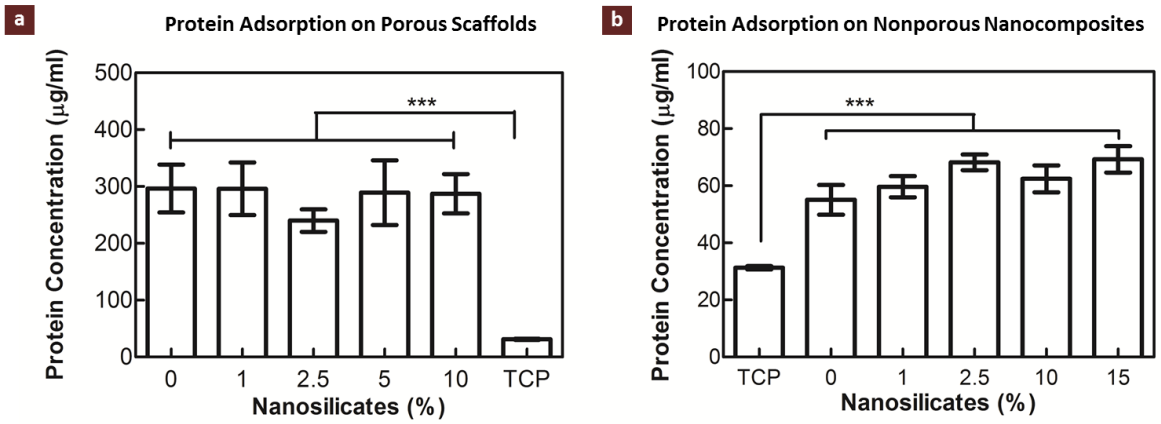

Figure III.6 Protein adsorption and cell adhesion on PGS/nanosilicates scaffolds. (a) Nanosilicate concentration had no statistically significant effects on protein adsorption on the scaffolds. It was obvious that the amount of protein adsorbed on the scaffolds were significantly higher than that on TCP. This could be combinatorial effects of porosity and surface properties of the scaffolds. (b) Our previous study showed that non-porous PGS and PGS-nSi nanocomposites displayed greater protein adsorption compared to TCP. Also, the amount of protein adsorbed on the porous scaffolds was approximately 5 times higher than those on their solid counterparts.

III.3.4 PGS/Nanosilicates Scaffolds Were Protein Adhesive

When the scaffolds come into contact with physiological mediums, it is believed that the initial event is protein adsorption. The adsorbed protein layer will influence the subsequent biological responses including cell adhesion and migration.[52] As proteins are viewed as primary players in mediating material-cell interactions, protein adsorption on PGS/nanosilicates scaffolds was investigated along with the cellular studies. Fetal bovine serum (FBS) was used for protein adsorption study as it was a component of cell culture media. After 24 hours, concentration of FBS adsorbed on the scaffold surface

was measured using micro BCA assay. The results showed that protein adsorption on the scaffolds was significantly higher than that on TCP control, and there was no statistically significant difference between scaffold compositions (figure III.6a). On average, proteins adsorbed on the scaffolds were approximately 9 times higher than that on TCP. This might have been expected since porous scaffolds had greater surface area than TCP. Nevertheless, our previous studies with nonporous PGS/nanosilicates nanocomposites revealed that protein adsorption on the nanocomposite's surface were twice the amount on TCP (figure III.6b). Considering that nanosilicates had no statistical significant effects on protein adsorption and the increases were also observed on nonporous nanocomposites, it was likely that surface properties of PGS itself could promote protein adsorption.

3.5 PGS/Nanosilicates Scaffolds Enhanced Cell Adhesion and Supported Cell Proliferation

The scaffolds seeded with MC-3T3 preosteoblasts were imaged with SEM in order to investigate cell adhesion and morphology. All scaffolds (both PGS and PGS/nanosilicates) were found to well support cell adhesion. Remarkably, the addition of nanosilicates resulted in increased cell spreading, and the increases were more prominent in normal growth media as compared to osteoconductive media (figure III.7a). This could be attributed to the presence of nanosilicates or enhanced surface stiffness, or their combinatorial effects. Our earlier works showed that the addition of nanosilicates to non-fouling and cell resistant surfaces (polyethylene glycol (PEG) and PNIPAM) greatly enhanced cell adhesion and spreading in a concentration-dependent manner.[43-47] It was hypothesized that nanosilicates provided sites for protein adsorption and subsequent cell adhesion. This hypothesis might controvert the results showing that nanosilicates had no statistically significant effects on the number of proteins adsorbed on the scaffolds (figure III.6). Nevertheless, the actual mechanisms underlying increased cell spreading upon the addition of nanosilicates are still unclear. Furthermore, increased cell spreading has been reported to promote osteogenic

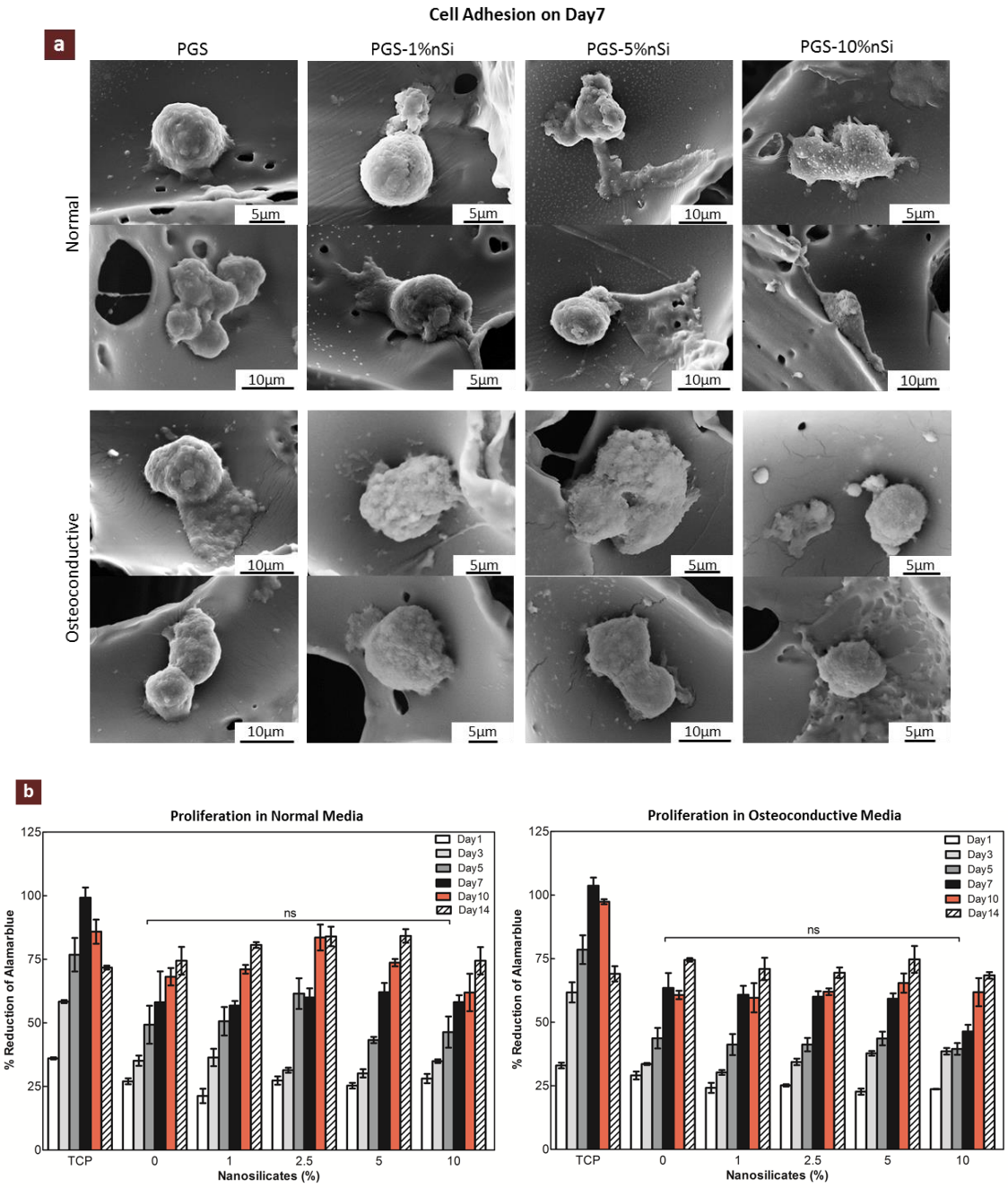

Figure III.7 Cell adhesion and proliferation. (a) SEM images of preosteoblasts after 7 days in culture showed well-adhered cells on the scaffolds. Cell adhesion/spreading was found to increase with increasing nanosilicate content; and the cells cultured in osteoconductive media spread more than those in normal growth media. It should be noted that increased spreading of bone progenitor cells was reported in literature to correlate with osteogenic differentiation. (b) AlamarBlue® assay showed that both PGS and PGS/nanosilicates scaffolds supported proliferation of preosteoblasts, suggesting their biocompatibility. There was no statistical difference between scaffolds compositions.

differentiation while suppressing adipogenic differentiation of mesenchymal stem cells (MSCs). This could be due to enhanced cytoskeletal contractility with increased cell spreading, and high contractility was found to correlate with osteogenesis.[50, 53] Thus, we hypothesized that the enhanced cell spreading on PGS/nanosilicates scaffolds would favor osteogenic differentiation.

Metabolic activity of seeded preosteoblasts was studied over two weeks using alamarBlue® assay (figure III.7b). All PGS and PGS-nanosilicates scaffolds were found to support cell proliferation. Metabolic activity of the cells increased over time, except for TCP that the activity started to decrease after 10 days. The decline could be attributed to the cells reaching confluency which was not observed on the scaffolds possessing higher surface area. There was no statistically significant difference in cell proliferation between scaffold compositions; and the trends were the same for both culture mediums. The results suggested cytocompatibility of nanosilicates as well as the scaffolds. As mentioned earlier, nanosilicates were reported to be cytotoxic at ten-fold higher concentration comparing to silica nanoparticles and the widely used nanohydroxyapatite.[15] Also, PGS is biocompatible and its degradation products are often metabolized in the body.[33]

AlamarBlue® assay showed that nanosilicates had no significant effects on preosteoblast proliferation. This opposed the previous reports that the addition of nanosilicates to polyethylene oxide (PEO) increased cell metabolic activity in a concentration-dependent manner.[44] The discrepancy could be attributed to the low cell-adherent surface of PEO. Since PEO exhibited low cell attachment, significant enhancement in cell adhesion and proliferation was observed upon the addition of nanosilicates. On the other hand, PGS itself is cell adhesive and has been demonstrated in literature to support cell proliferation. Particularly, cell proliferation on PGS solid substrates was found to be slightly slower than that on TCP, whereas metabolic activity of cells on PEO-nanosilicates systems was still significantly lower than that on TCP even with 70% nanosilicates addition.[50]

Cross-section SEM images of the seeded scaffolds after 7 days in culture showed limited cell migration down the pores (data not shown). After thorough inspection, limited pore connectivity was likely to be the cause. This could be improved by particulate fusion method where the porogens would be fused together in a humidity chamber before used as a template for solvent casting. This fabrication technique should create a more open porous structure. The extensive micropores resulted from salt-fusion should increase mass transfer as well as cellular communication, and facilitate the formation of 3D tissue construct.

III.3.6 PGS/Nanosilicates Scaffolds Promoted Osteogenic Differentiation

The ability of PGS/nanosilicates scaffolds to promote osteogensis was determined by assessing alkaline phosphatase (ALP) activity and matrix mineralization of seeded MC-3T3 preosteoblasts. The studies were conducted in both normal growth media and osteoconductive media (α-MEM supplemented with β-glycerophosphate and ascorbic acid). ALP activity, an early marker of osteogenic differentiation, was examined after 7 days in culture. ALP staining by BCIP/NBT together with quantitative analysis of ALP/dsDNA showed increased ALP activity upon the addition of nanosilicates; and the enhancement was more prominent in osteoconductive media (figure III.8). The increases could be seen even when the cells were cultured in normal growth media without any osteogenic supplements.

In addition, matrix mineralization, a late-stage marker of osteogenic differentiation, was assessed on day 14 by ARS staining and subsequent quantification. All scaffolds were stained bright red (figure III.9a). However, since they were all highly stained, the differences between compositions could not be observed from the images. ARS quantification clearly showed increased matrix mineralization with increasing nanosilicate concentration (figure III.9b). The enhancement was apparent in both normal growth media and osteconductive media. For example, the addition of 10% nanosilicates gave rise to almost 3 times increase in normal growth media and over 1.5 times increase in osteoconductive media. For all scaffold compositions, degree of osteogenic

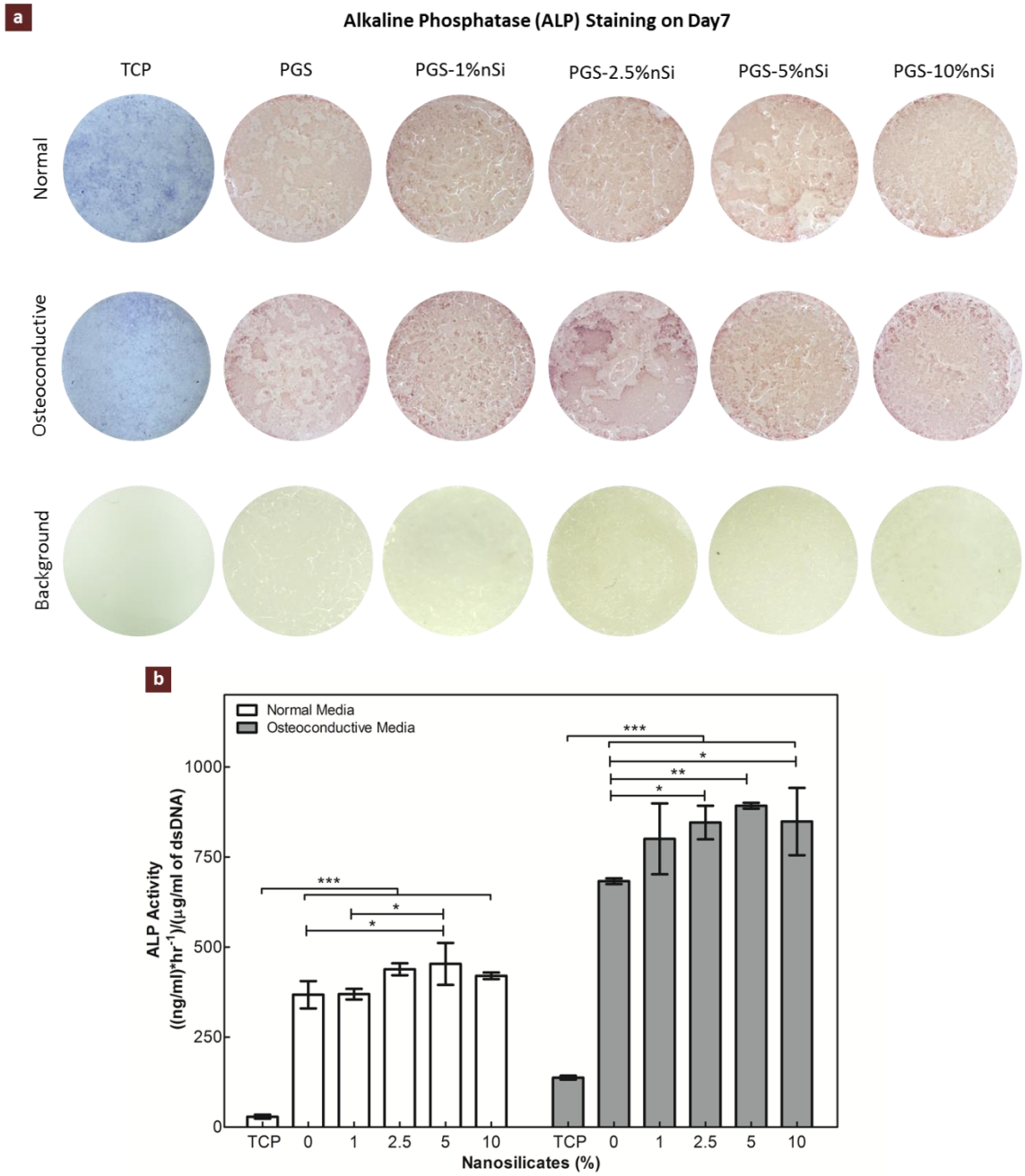

Figure III.8 Alkaline phosphatase (ALP) expression. ALP is an early marker of osteogenic differentiation. After 7 days in culture, seeded TCP and scaffolds displayed blue/purple staining. There was slightly more ALP staining on PGS-nSi than on PGS only scaffolds; however, the increases could not be clearly observed from the images. (b) Further quantification showed increased ALP activity per DNA upon the addition of nanosilicates; and the enhancement was more prominent in osteoconductive media. It should

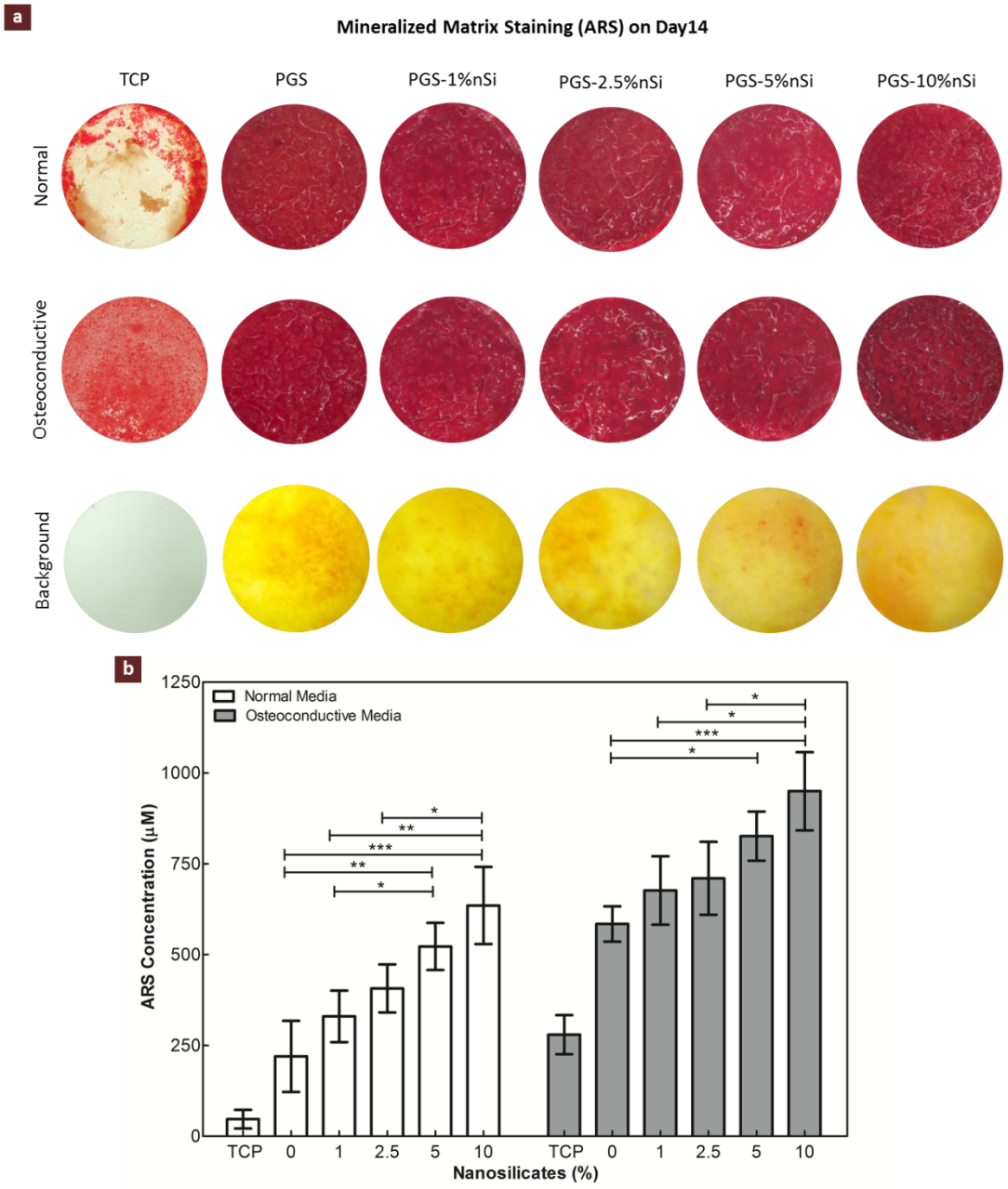

Figure III.9 Matrix mineralization. Matrix mineralization is a late marker of osteogenic differentiation. (a) After 14 days in culture, seeded TCP and scaffolds were stained bright red by Alizarin Red S (ARS). There was more mineralization in osteocondutive media than in normal media as evidence on the TCP. However, since the scaffolds extensively adsorbed ARS, differences between compositions could not be observed from the images. (b) Further quantification clearly showed that the mineralization increased with increasing nanosilicate concentration, in both normal and osteconductive medias. Enhancement of ALP activity (figure6) and matrix mineralization upon the addition of nanosilicates in normal growth media indicated that the material could promote osteogenic differentiation in the absence of any osteogenic factors.

differentiation was higher in osteoconductive media than in normal growth media as expected. Remarkably, enhancement of ALP activity and matrix mineralization upon the addition of nanosilicates indicated a key role of nanosilicates in upregulating osteogenic differentiation. The apparent increases when cultured in normal growth media suggested osteoinductive properties of nanosilicates as previously reported. Osteoinduction capability of nanosilicates will offer growth-factor-free approach for bone regeneration which could minimize expense and complexity involved in growth factor delivery.

III.4 SUMMARY

We successfully fabricated porous nanocomposite scaffolds of PGS/nanosilicates. The addition of nanosilicates resulted in increased physical integrity as well as enhanced mechanical strength and toughness without compromising elastomeric properties, the mechanical characteristics that would provide load-transducing environment for bone regeneration. The achieved mechanical properties looked promising for craniofacial defect reconstruction. In the future, we aim to increase nanosilicate contents to obtain compressive modulus and toughness closer to that of trabecular bone. The scaffolds supported preosteoblast proliferation and increased cell adhesion and spreading into the morphology reported to favor osteogenic differentiation. The addition of nanosilicates could promote osteogenic differentiation in the absence of osteogenic factors, suggesting osteoinductive properties of the scaffolds. Overall, the results showed that PGS/nanosilicates nanocomposites are promising for growth-factor-free bone tissue engineering.

CHAPTER IV

CONCLUSIONS

Our long-term goal is to develop three-dimensional scaffold that possesses intrinsic osteoinductivity, allows the formation of three-dimensional tissue construct, and have tailorable mechanical properties and degradation kinetic, so that it provide load-transducing environment suitable for bone regeneration. The objective of this thesis project is to design porous nanocomposite scaffold from 2D nanosilicates and PGS. The central hypothesis is that PGS/nanosilicates scaffolds will promote osteogenic differentiation of seeded progenitor cells, and have tunable mechanical properties. The rational underlying this project is that there is yet no bone scaffold that is both osteinductive and provides optimal mechanical environment for bone engineering. It is well established that these two characteristics are of atmost importance for proper bone repair and anchorage of the graft. Therefore, we would like to develop scaffold that can overcome these two main challenges.

Since it was the first time nanocomposites of PGS and nanosilicates were made, we first investigated effects of nanosilicate concentration on various properties including hydration, thermal, mechanical, and degradation properties. Then, we evaluated their potential for bone tissue engineering application by assessing in vitro bioactivity, protein adhesion, and cellular responses of seeded MC-3T3 preosteoblasts. As the results were promising, porous PGS/nanosilicates scaffolds were fabricated via salt leaching technique.

The addition of nanosilicates increased hydrophilicity and crosslinking density in a concentration-dependent manner. The increased crosslinking gave rise to enhanced physical and thermal stability, as well as mechanical strength and toughness. This was mainly attributed to interactions between nanosilicates and polymer matrix, and the fact that nanosilicates served as network crosslinkers. In particular, nanosilicates

significantly retarded degradation of nanocomposites and scaffolds. SEM images showed minimal changes in surface morphology upon the addition of 10% nanosilicates to the nanocomposites. The nanocomposite scaffolds exhibited surface-eroding degradation which is preferable over other bulk-degrading polyester scaffolds as they can better maintain structural integrity while the scaffold is being replaced by newly formed bone. Remarkably, the addition of nanosilicates enhanced mechanical strength and toughness without compromising elastomeric properties. These mechanical characteristics were promising as the scaffolds would provide load-transducing environment for bone repair. In the future, we can increase nanosilicate content to bring the mechanical strength closer to that of trabecular bone.

Furthermore, in vitro bioactivity was found to be increased upon the addition of nanosilicates. The nanocomposite scaffolds supported cell proliferation and promoted cell spreading to the morphology reported to be favorable for osteogenic differentiation. The addition of nanosilicates enhanced osteogenic differentiation of seeded preosteoblasts as evidenced by increased ALP activity and matrix mineralization. The enhancement could be observed even when the seeded scaffolds were culture in normal growth media without any osteogenic factor. These results suggested osteoinductive capability of the scaffolds which offered a growth-factor-free approach for bone tissue engineering.

However, one remaining challenge of the fabricated scaffolds was inefficient pore interconnectivity. This resulted in limited cell penetration down the pores and consequently the formation of 3D tissue construct. In the future, this could be improved by combining particulate fusion technique with salt leaching method. This integrative technique has been demonstrated to create higher pore interconnectivity and more open structure. The extensive micropores resulted from salt-fusion should increase mass transfer as well as cellular communication, and facilitate the formation of 3D tissue construct.

REFERENCES

[1] Giannoudis PV, Dinopoulos H, Tsiridis E. Bone Substitutes: An Update. Injury, Int J Care Injured 2005;36S:S20-S7.

[2] Grabowski G, Cornett CA. Bone Graft and Bone Graft Substitutes in Spine Surgery: Current Concepts and Controversies. Journal of the American Academy of Orthopaedic Surgeons 2013;21:51-60.

[3] Pape HC, Evans A, Kobbe P. Autologous Bone Graft: Properties and Techniques. Journal of Orthopaedic Trauma 2010;24:S36-S40.

[4] Marino JT, Ziran BH. Use of Solid and Cancellous Autologous Bone Graft for Fractures and Nonunions. Orthopedic Clinics of North America 2010;41:15-26.

[5] Kneser U, Schaefer DJ, Polykandriotis E, Horch RE. Tissue Engineering of Bone: The Reconstructive Surgeon's Point of View. Journal of Cellular and Molecular Medicine 2006;10:7-19.

[6] Bohner M. Resorbable Biomaterials as Bone Graft Substitutes. Materials Today 2010;13:20-30.

[7] Greenwald AS, Dphil(Oxon), Boden SD, Goldberg VM, khan Y, Laurencin CT, et al. Bone-graft Substitutes: Facts, Fictions, and Applications. The Journal Of Bone And Joint Surgery 2001;83:98-103.

[8] Blokhuis TJ, Arts JJC. Bioactive and Osteoinductive Bone Graft Substitutes: Definitions, Facts and Myths. Injury 2011;42 S26-S9.

[9] Jones JR. Review of Bioactive Glass: From Hench to Hybrids. Acta Biomaterialia 2013;9:4457–86.

[10] Seebachemail C, Schultheiss J, Wilhelm K, Frank J, Henrich D. Comparison of Six Bone-graft Substitutes Regarding to Cell Seeding Efficiency, Metabolism and Growth Behaviour of Human Mesenchymal Stem Cells (MSC) In Vitro. Injury 2010;41:731–8.

[11] Albrektsson T, Johansson C. Osteoinduction, Osteoconduction and Osseointegration. European Spine Journal 2001;10:S96-S101.

[12] Valliant EM, Jones JR. Softening Bioactive Glass for Bone Regeneration: Sol–gel Hybrid Materials. Soft Matter 2011;7:5083-95.

[13] Moore WR, Graves SE, Bain GI. Synthetic Bone Graft Substitutes. ANZ Journal of Surgery 2001;71:354-61.

[14] Detsch R, Mayr H, Ziegler G. Formation of Osteoclast-like Cells on HA and TCP Ceramics. Acta Biomaterialia 2008;4:139-48.

[15] Gaharwar AK, Mihaila SM, Swami A, Patel A, Sant S, Reis RL, et al. Bioactive Silicate Nanoplatelets for Osteogenic Differentiation of Human Mesenchymal Stem Cells. Advanced Materials 2013;25:3329–36.

[16] Mihaila SM, Gaharwar AK, Reis RL, Khademhosseini A, Marques AP, Gomes ME. The Osteogenic Differentiation of SSEA-4 Sub-population of Human Adipose Derived Stem Cells Using Silicate Nanoplatelets. Biomaterials 2014;35:9087-99.

[17] Hoppe A, Güldal NS, Boccaccini AR. A Review of the Biological Response to Ionic Dissolution Products From Bioactive Glasses and Glass-ceramics. Biomaterials 2011;32:2757-74.

[18] Zreiqat H, Howlett CR, Zannettino A, Evans P, Schulze-Tanzil G, C. Knabe MS. Mechanisms of Magnesium-stimulated Adhesion of Osteoblastic Cells to Commonly Used Orthopaedic Implants. Journal of Biomedical Materials Research 2002;62:175–84.

[19] Kubota T, Michigami T, Ozono K. Wnt Signaling in Bone Metabolism. J Bone Miner Metab 2009;27:265–71.

[20] Reffitt DM, Ogston N, Jugdaohsingh R, Cheung HFJ, Evans BAJ, Thompson RPH, et al. Orthosilicic Acid Stimulates Collagen Type 1 Synthesis and Osteoblastic Differentiation in Human Osteoblast-like Cells In Vitro. Bone 2003;32:127–35.

[21] Gaharwar AK, Peppas NA, Khademhosseini A. Nanocomposite Hydrogels for Biomedical Applications. Biotechnology and Bioengineering 2014;111:441-53.

[22] Carrow JK, Gaharwar AK. Bioinspired Polymeric Nanocomposites for Regenerative Medicine. Macromolecular Chemistry and Physics 2015;216:248-64.

[23] Podsiadlo P, Kaushik AK, Arruda EM, Waas AM, Shim BS, Jiadi Xu HN, et al. Ultrastrong and Stiff Layered Polymer Nanocomposites. Science 2007;318:80-3.

[24] Gaharwar AK, Rivera CP, Wu C-J, Schmidt G. Transparent, Elastomeric and Tough Hydrogels from Poly(ethylene glycol) and Silicate Nanoparticles. Acta Biomaterialia 2011;7:4139–48.

[25] Bonderer LJ, Studart AR, Gauckler LJ. Bioinspired Design and Assembly of Platelet Reinforced Polymer Films. Science 2008;319:1069-73

[26] Gaharwar AK, Schexnailder P, Kaul V, Ozan Akkus, Zakharov D, Seifert S, et al. Highly Extensible Bio-Nanocomposite Films with Direction-Dependent Properties. Advanced Functional Materials 2010;20:429–36.

[27] Haraguchi K. Synthesis and Properties of Soft Nanocomposite Materials with Novel Organic/inorganic Network Structures. Polymer Journal 2011;43:223–41.

[28] Gaharwar AK, Avery RK, Assmann A, Paul A, McKinley GH, Khademhosseini A, et al. Shear-Thinning Nanocomposite Hydrogels for the Treatment of Hemorrhage. ACS Nano 2014;8:9833–42.

[29] Wang Q, Mynar JL, Yoshida M, Lee E, Lee M, Okuro K, et al. High-water-content Mouldable Hydrogels by Mixing Clay and a Dendritic Molecular Binder. Nature 2010;463:339-43.

[30] Dawson JI, Kanczler JM, Yang XB, Attard GS, Oreffo ROC. Clay Gels For the Delivery of Regenerative Microenvironments. Advanced MAterials 2011;23:3304–8.

[31] Dawson JI, Oreffo ROC. Clay: New Opportunities for Tissue Regeneration and Biomaterial Design. Advanced Materials 2013;25:4069–86.

[32] Xavier JR, Thakur T, Desai P, Jaiswal MK, Sears N, Cosgriff-Hernandez E, et al. Bioactive Nanoengineered Hydrogels for Bone Tissue Engineering: A Growth-Factor-Free Approach. ACS Nano 2015;9:3109–18.

[33] Rai R, Tallawi M, Grigore A, Boccaccini AR. Synthesis, Properties and Biomedical Applications of Poly(glycerol sebacate) (PGS): A Review. Progress in Polymer Science 2012;37:1051– 78.

[34] Wang Y, Kim YM, Langer R. In Vivo Degradation Characteristics of Poly(glycerol sebacate). Journal of Biomedical Materials Research Part A 2003;66A:192-7.

[35] Wang Y, Ameer GA, Sheppard BJ, Langer1 R. A Tough Biodegradable Elastomer. Nature Biotechnology 2002;20:602-6.

[36] Gaharwar AK, Patel A, Dolatshahi-Pirouz A, Zhang H, Rangarajan K, Iviglia G, et al. Elastomeric Nanocomposite Scaffolds Made from Poly(glycerol sebacate) Chemically Crosslinked with Carbon Nanotubes. Biomaterials Science 2015;3:46-58.

[37] Zaky SH, Lee K-W, Gao J, Jensen A, Close J, Wang Y, et al. Poly(Glycerol Sebacate) Elastomer: A Novel Material for Mechanically Loaded Bone Regeneration. Tissue Engineering: Part A 2014;20:45-53.

[38] Zaky SH, Hangadora CK, Tudares MA, Gao J, Jensen A, Wang Y, et al. Poly (glycerol sebacate) Elastomer Supports Osteogenic Phenotype for Bone Engineering Applications. Biomed Mater 2014;9:025003.

[39] Deng Y, Bi X, Zhou H, You Z, Wang Y, Gu1 P, et al. Repair of Critical-Sized Bone Defects with Anti-MIR-31-Expressing Bone Marrow Stromal Stem Cells and Poly(glycerol sebacate) Scaffolds. European Cells and Materials 2014;27:13-25.

[40] Tas AC, Bhaduri SB. Rapid coating of Ti6Al4V at room temperature with a calcium phosphate solution similar to 10× simulated body fluid. J Mater Res 2004;19:2742-49.

[41] Patel A, Gaharwar AK, Iviglia G, Zhang H, Mukundan S, Mihaila SM, et al. Highly Elastomeric Poly(glycerol sebacate)-co-Poly(ethylene glycol) Amphiphilic Block Copolymers. Biomaterials 2013;34:3970–83.

[42] Kokubo T, Takadama H. How useful is SBF in predicting in vivo bone bioactivity? Biomaterials 2006;27:2907–15.

[43] Schexnailder PJ, Gaharwar AK, Bartlett RL, Seal BL, Schmidt G. Tuning Cell Adhesion by Incorporation of Charged Silicate Nanoparticles as Cross-Linkers to Polyethylene Oxide. Macromol Biosci 2010;10:1416–23.

[44] Gaharwar AK, Kishore V, Rivera C, Whitney Bullock, Wu C-J, Akkus O, et al. Physically Crosslinked Nanocomposites from Silicate-Crosslinked PEO: Mechanical Properties and Osteogenic Differentiation of Human Mesenchymal Stem Cells. Macromol Biosci 2012;12:779–93.

[45] Gaharwar AK, Schexnailder PJ, Kline BP, Schmidt G. Assessment of using Laponite cross-linked poly(ethylene oxide) for controlled cell adhesion and mineralization. Acta Biomaterialia 2011;7:568–77.

[46] Gaharwar AK, Schexnailder P, Kaul V, Ozan Akkus, Zakharov D, Seifert S, et al. Highly Extensible Bio-Nanocomposite Films with Direction-Dependent Properties. Adv Funct Mater 2010;20:429–36.

[47] Dawson JI, Oreffo ROC. Clay: New Opportunities for Tissue Regeneration and Biomaterial Design. Adv Mater 2013;25:4069–86.

[48] Xavier JR, Thakur T, Desai P, Jaiswal MK, Sears N, Cosgriff-Hernandez E, et al. Bioactive Nanoengineered Hydrogels for Bone Tissue Engineering: A Growth-Factor-Free Approach. ACS Nano 2015;9:3109-18.

[49] Gao J, Crapo PM, Wang Y. Macroporous Elastomeric Scaffolds with Extensive Micropores for Soft Tissue Engineering. Tissue Engineering 2006;12:917-25.

[50] Kerativitayanan P, Gaharwar AK. Elastomeric and mechanically stiff nanocomposites from poly(glycerol sebacate) and bioactive nanosilicates. Acta Biomaterialia 2015;26:34-44.

[51] Chen Q-Z, Quinn JMW, Thouas GA, Zhou X, Komesaroff PA. Bone-Like Elastomer-Toughened Scaffolds with Degradability Kinetics Matching Healing Rates of Injured Bone. Advanced Engineering Materials 2012;12:B642-B8.

[52] Chen H, Yuan L, Song W, Wu Z, Li D. Biocompatible Polymer Materials: Role of Protein–Surface Interactions. Progress in Polymer Science 2008;33:1059–87.

[53] Song W, Kawazoe N, Chen G. Dependence of Spreading and Differentiation of Mesenchymal StemCells onMicropatterned Surface Area. Journal of Nanomaterials 2011;265251.